molecules

MDPI

Review

A Review on the Recent Advancements of Ni-Based Sulfides and Mixed Sulfides for Supercapacitors and Electrocatalysis (Oxygen Evolution Reaction)

Ganesh Dhakal [1,*], Sumanta Sahoo [2,*], Krishna Prasad Sharma [1] and Guang-Lin Zhao [1,*]

[1] Department of Physics and Nano Materials Laboratory, Southern University and A&M College, Baton Rouge, LA 70813, USA
[2] School of Chemical Engineering, Yeungnam University, 280 Daehak-ro, Gyeongsan 38541, Republic of Korea
* Correspondence: ganesh.dhakal@sus.edu (G.D.); sumanta95@gmail.com (S.S.); guang-lin.zhao@sus.edu (G.-L.Z.)

Abstract

Energy storage and conversion units have been considered the backbone of modern energy science and technology. In recent years, the Ni-based sulfides (NS) and mixed sulfides (NMS) have been significantly utilized as promising electrodes for various energy-related applications. This article summarizes the recent progress of NS and NMS materials in the fields of energy storage (supercapacitors) and conversion (oxygen evolution reactions). The synthetic approaches have been thoroughly discussed. A brief overview of the electrochemical performance of these materials as the electrodes for energy storage and conversion is systematically represented in the article. For such applications, these materials are frequently combined with other advanced materials, such as metal oxides, metal sulfides, and carbonaceous materials. The article ends with the existing challenges and future research directions in these research fields.

Keywords: nickel sulfide; nickel mixed sulfide; supercapacitor; oxygen evolution reaction

check for updates

Academic Editor: César Augusto Correia de Sequeira

Received: 6 June 2025
Revised: 1 July 2025
Accepted: 4 July 2025
Published: 7 July 2025

Citation: Dhakal, G.; Sahoo, S.; Sharma, K.P.; Zhao, G.-L. A Review on the Recent Advancements of Ni-Based Sulfides and Mixed Sulfides for Supercapacitors and Electrocatalysis (Oxygen Evolution Reaction). *Molecules* **2025**, *30*, 2877. https://doi.org/10.3390/molecules30132877

Copyright: © 2025 by the authors. Licensee MDPI, Basel, Switzerland. This article is an open access article distributed under the terms and conditions of the Creative Commons Attribution (CC BY) license (https://creativecommons.org/licenses/by/4.0/).

1. Introduction

Electrochemical energy storage and conversion systems have been considered as the pioneer technology of the current century. The storage of energy and its conversion from one form to another through electrochemical processes has drawn considerable research attention because of their easy processability, diverse range of applications, and huge demand for future technology. In this aspect, the energy storage devices, like secondary batteries and supercapacitors (SCs), have been considered as the key devices [1–5]. On the other hand, the oxygen evolution reaction (OER) is assigned as the vital component for constructing the energy conversion [6–10]. Such components not only advance future technology but also promote renewable energy resources, which further leads to the formation of a green and sustainable future.

Metal oxides and mixed metal oxides have been synthesized through diverse synthetic routes for constructing energy electrodes. Specifically, the transition metal oxides/mixed oxides demonstrated superior supercapacitive performance over their other metal counterparts [11–13]. Significant research has also been conducted in the case of metal sulfides and mixed metal sulfides. These materials display higher electrochemical characteristics over their oxide counterparts because of richer surface chemistry, enhanced conductive nature, and higher electronic properties. Compared to other transition metals, Ni has the

advantages of richer redox activity, tunable structure and composition, better stability, lower cost, and higher abundance. Among transition metals, Ni is considered a potential component for fabricating energy electrodes due to its favorable electrochemical activity. In this aspect, the Ni-based metal oxide (NiO) and mixed oxide ($NiCo_2O_4$) have been widely investigated [14–16]. In the last few years, Ni-based sulfides (NS) and mixed sulfides (NMS) have been extensively investigated for developing electrodes for energy storage and conversion [17–21]. In order to improve the performance, such materials have further been combined with other metal sulfides/mixed sulfides, metal oxides/mixed oxides, carbon materials, MXenes, conducting polymers, etc. [22–24].

The current article reviews the most recent advancements of NS and NMS in the field of energy storage (SC) and conversion (OER). The research investigations of these materials in the last 5 years (2020–2025) are thoroughly discussed. The article starts with a brief introduction to the above-mentioned energy storage and conversion applications. The synthetic approaches are further summarized. Lastly, the article ends with the conclusion and future prospects. Figure 1 represents the prime aim of the review article. As shown, the NS and NMS materials have been frequently utilized for energy-related applications because of their high surface area, enhanced porosity, rich redox activity, easy synthetic approaches, high catalytic activity, and natural abundance.

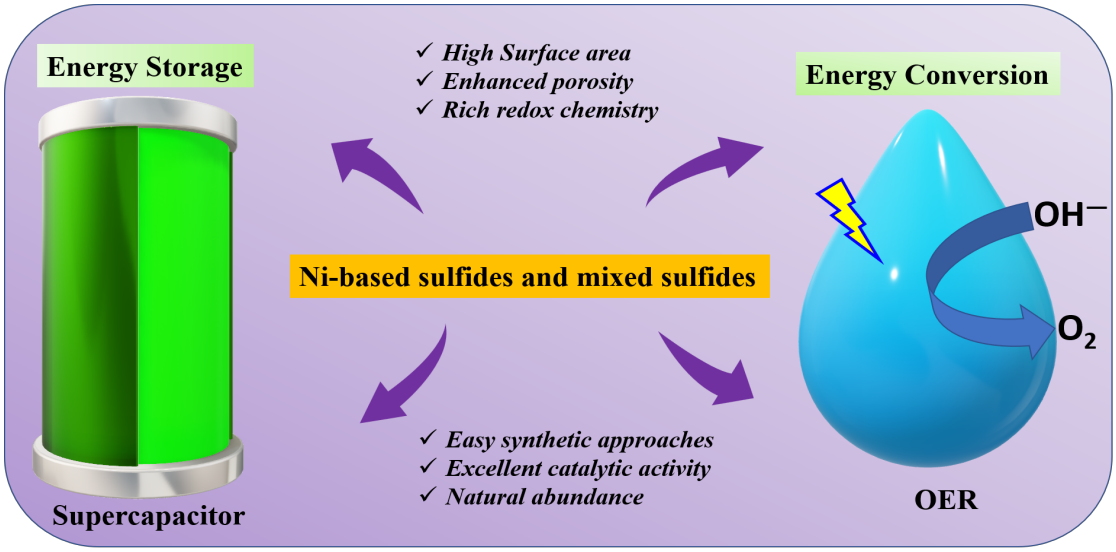


Figure 1. Schematics of the aim of the current review article, highlighting the advantages of Ni-based sulfide and mixed sulfide materials.

2. Brief Discussion on Energy Storage and Conversion

Energy storage and conversion of one form to another have become crucial for the development of a sustainable world. Specifically, renewable energy resources have been considered as valuable assets of modern science and technology. Among the energy storage devices, SCs are considered promising because of their fast charge–discharge ability, longer cycle life, and easy fabrication processes. According to the charge storage mechanism, such devices are classified into two classes: pseudocapacitive (store charge through Faradaic reactions) and electric-double-layer capacitors (EDLC) (store charge through a non-Faradaic fashion) [1,25–27]. A great deal of research has been conducted on the synthesis of the SC electrodes. The carbon-based materials generally store charges through the EDLC charge storage mechanism [28–30]. On the other hand, the metal oxides, metal chalcogenides, conductive polymers, etc., follow the pseudocapacitive charge storage mechanism [31–34]. It is important to note that the electrochemical performance of SC electrodes depends on several factors, including the surface area, porosity, conductivity, and crystallinity of

the electrode materials. On the other hand, the electrolytes also play a significant role in the performance of the SCs. The concentration, ionic conductivity, and nature of the electrolytes expressively influence the charge–storage ability of the electrodes. For example, a previous report demonstrated the increment of capacitance of an SC electrode based on $NiCo_2O_4$ by enhancing the concentration of KOH electrolyte [35]. The combination of pseudocapacitive and EDLC-type materials produces the hybrid SC electrodes, which are nothing but composite-type materials. These materials are constructed to utilize the advantages of both the pseudocapacitor and EDLC. The SC devices are constructed by combining the positive and negative electrode materials. In general, the carbon-based materials, like activated carbon, graphene, etc., are being utilized as the negative electrodes. The current research trend in SC has moved towards the exploration of sustainable resources for the fabrication of electrodes. In this context, the biomass-derived carbon materials have been considered as the pioneer materials for SCs.

Electrochemical water splitting (EWS) is an efficient method for producing hydrogen and oxygen by breaking down water molecules through the hydrogen evolution reaction (HER) and OER [6–8,10,36]. Although the theoretical cell voltage essential for water splitting is 1.23 V, in practice, a higher voltage, known as overpotential (OP), is needed to drive the reaction efficiently. To reduce this OP and improve overall efficiency, effective and affordable electrocatalysts are essential. Precious metal-based catalysts such as platinum (Pt) and ruthenium oxide (RuO_2) have been used for HER and OER and have demonstrated excellent catalytic performance. However, their high cost, limited availability, and environmental concerns restrict their large-scale and long-term use. Therefore, there is a growing need to develop low-cost, abundant, and green alternative electrocatalysts to make water splitting. The selection of the electrocatalysts highly affects the water splitting performance. Additionally, the stability and efficiency of these materials also influence the overall catalytic activity. Extensive research has been conducted on the development of electrocatalysts for water splitting, focusing on a wide range of materials, including transition metal oxides, sulfides, phosphides, nitrides, and carbon-based compounds [37,38]. Among these, transition metal sulfide-based electrocatalysts have gained significant attention due to their excellent catalytic activity, natural abundance, cost-effectiveness, and high surface area. These properties make them promising alternatives to traditional Pt-based catalysts, which, although highly efficient, are expensive and scarce.

3. Synthetic Approaches

The NS and NMS materials have been extensively synthesized through versatile synthetic approaches. Among them, the most common synthetic approach is the hydrothermal process. It is important to note that such a specific synthetic route has not only been employed for synthesizing NS and NMS-based powder materials but also explored to grow such materials in various conductive substrates; for example, Ni foam (NF). In this aspect, Yan et al. reported the hydrothermal synthesis of NiS nanosheets on NF [39]. In a typical process, the Ni-based salt, $Ni(NO_3)_2$, along with urea and NF, was hydrothermally treated at 180 °C for 18 h at a heating rate of 3 °C/min. In the next step, the coated foam was further hydrothermally heated at 120 °C for 3 h along with Na_2S, which was used as the S-source. The morphological analysis confirmed the growth of NiS nanosheets. In another work, β-NiS was hydrothermally synthesized using $Ni(CH_3COO)_2{\cdot}4H_2O$ salt [40]. However, in this case, the reaction temperature was set at 150 °C for a reaction time of 12 h for the synthesis of metal sulfide nanoparticles. The hydrothermal synthetic approaches associated with the post-heat treatment are reported for synthesizing various NS-based materials with diverse morphologies and related composites. The metal–organic framework (MOF)-derived NS materials have also been synthesized through this approach. In this

aspect, Wang et al. demonstrated the hydrothermal-assisted synthesis of an MOF-derived NiS/NiS_2@carbon composite, as shown in Figure 2 [41]. For the MOF synthesis, 3,3′,5,5′-azobenzenetetracarboxylic acid (H_4ABTC) was used, and the MOF-derived NS material was synthesized through pyrolysis at 500 °C in an Ar atmosphere. Hydrothermal synthesis was further employed for the synthesis of the composite based on Cu_2S, NiS, Ni_3S_4, and MnO_2 [42]. In another work, P-doped Co_3S_4 was combined with Ni_3S_4 on NF through a two-step hydrothermal approach, where NaH_2PO_2 was utilized as the doping agent in the phosphating method [43].

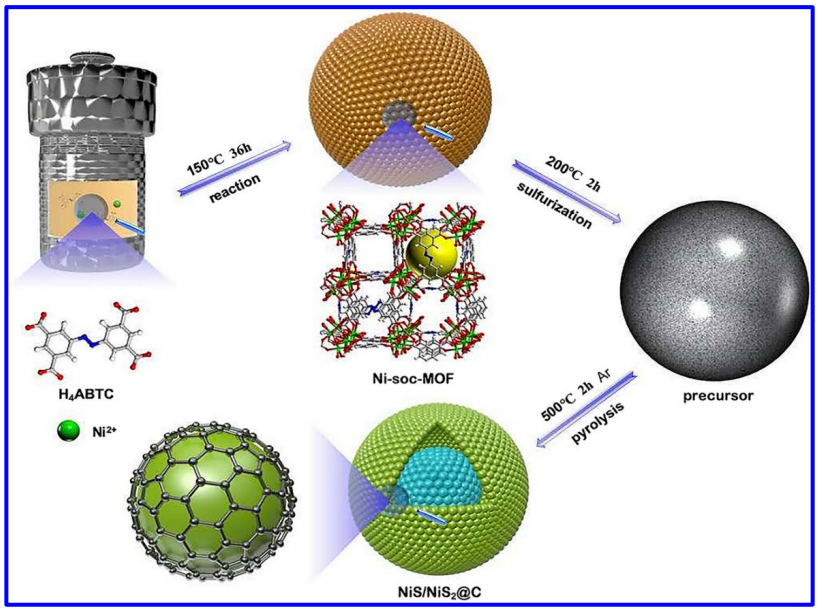


Figure 2. Schematics of the synthetic approach of NiS/NiS_2@carbon composite [41].

Apart from hydrothermal, the solvent-free direct synthesis of NiS with nanosheet morphology was reported [44]. In this process, Ni-containing salt, Ni $(CH_3COO)_2{\cdot}4H_2O$, $(NH_2)_2CS$, and NaCl were ground and further heat-treated at 120 °C for 12 h in a blast oven, resulting in the formation of graphene-like ultra-thin NiS nanosheets (Figure 3a). Herein, the addition of NaCl regulated the growth process and prevented the thickness of NiS nanosheets. The associated reactions are provided below:

$$Ni(CH_3COO)_2{\cdot}4H_2O \rightarrow Ni(CH_3COO)_2 + 4H_2O \quad (1)$$

$$(NH_2)_2CS + 2H_2O \rightarrow CO_2 + 2NH_3 + H_2S \quad (2)$$

$$Ni(CH_3COO)_2 + H_2S \rightarrow NiS + 2CH_3COOH \quad (3)$$

The formation of the final product after the heat treatment can be visualized with the naked eye through the transformation of the color from green (after grinding) to black. In another work, another solid-state synthetic approach was reported for the synthesis of both NiS and NiS_2 [45]. In this process, initially Ni formate and sulfur powder of the desired quantity were ground and calcined at a temperature of 440 °C for a reaction time of 30 min to synthesize the NiS_2 nanoparticles. The optimization of temperature resulted in the formation of NiS (Figure 3b). Compared to other conventional approaches, these solid-state processes have the advantages of the absence of hazardous chemicals and an easy synthetic protocol. In another work, a combination of the dealloying method and ion-exchange process resulted in the formation of NiS/NiO nanoparticles [46]. In this process, initially, the $Al_{91}Ni_9$ alloy was dealloyed, followed by a calcination process to form NiO. The further sulfuration process yielded a composite of NiO and NiS. The

solvent-free approaches were further employed in another work to synthesize α-NiS, β-NiS, and a combination of both types of NS materials [47]. In another work, a single-step electrodeposition process has been employed to synthesize a ternary composite based on Co_9S_8, NiS_2, and Cu_2S on NF [48]. In another work, a solvothermal synthetic route was conducted to synthesize Mg-MOF and Ni-MOF using terephthalic acid as the MOF precursor. Such MOFs have been utilized as precursors to form NS-based composites. In the next step, these precursors were hydrothermally treated along with Na_2S as the sulfur source to form the composite of $Mg(OH)_2$ and Ni_3S_4 [49]. The above-mentioned discussion concludes that the NS materials have been synthesized and subsequently combined with other potential functional materials for their utilization in the field of energy storage and conversion.

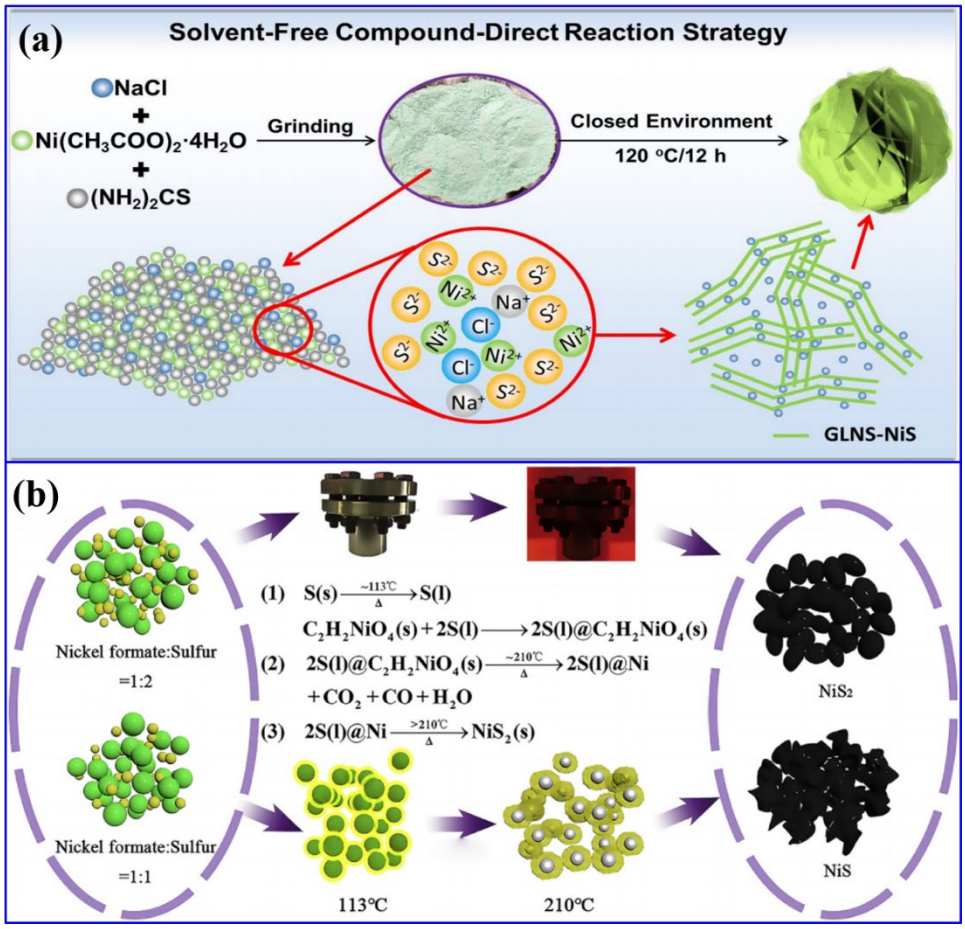


Figure 3. Solid-state synthesis of NS-based materials: (**a**) schematics of the solvent-free synthetic approach of graphene-like ultra-thin NiS nanosheets (GLNS-NiS) [44]; (**b**) schematics and the related reactions for the synthesis of NiS and NiS_2 [45].

Similar to the NS materials, NMS materials have also been frequently synthesized through the hydrothermal approach. Among the MNS materials, $NiCo_2S_4$ is the most-studied one for SC applications. In this aspect, Wang et al. demonstrated the hydrothermal synthesis of $NiCo_2S_4$ nanorods on NF (Figure 4a) [50]. In this approach, initially, the Ni and Co salts were hydrothermally treated along with urea at a temperature of 100 °C for 12 h to form the network-like structures of Ni-Co precursor. In the next step, the hydrothermal treatment (95 °C, 4 h) of the coated NF, along with thioacetamide (acting as the Sulfur source), resulted in the formation of the nanorods of $NiCo_2S_4$. The corresponding morphological images represent the formation of the nanorod arrays of the MNS material on the NF, as shown in the SEM images in Figure 4b–k. After the first hydrothermal

treatment, the interconnected networks of the Ni-CO precursors were formed (Figure 4b,c). The nanorod arrays of $NiCo_2S_4$ were formed after the second hydrothermal treatment for 2 h (Figure 4d,e). With an increase in the reaction time of 3 h, the diameter of the nanorods has been enhanced and, further, the tip of the rods became rougher (Figure 4f,g). At the reaction time of 4 h, the flower-like structure is visible (Figure 4h,i). Further increments in reaction time to 5 h resulted in the full blooming of the flowers (Figure 4j,k). During the first hydrothermal treatment, the urea acted as the hydrolyzing agent to produce the OH^- and CO_3^{2-} ions, which further reacted with the Ni^{2+} and Co^{2+} ions to form the Ni-Co precursor on NF. Further hydrothermal treatment with the S agent resulted in the formation of MNS materials through further reaction and an ion-exchange process. The sulfurization of the MNS material is also reported with a single-step hydrothermal process. In order to control the shape, surfactants have also been utilized. In this context, a recent report suggested a hydrothermal treatment of the nitrate salts of Ni and Co, urea, and $Na_2S{\cdot}9H_2O$, along with the hexamethylenetetramine (HMTA), which acted as the surfactant to form the nanosheets of $NiCo_2S_4$ [51]. Such hydrothermal processes have been further utilized to prepare the composite SC electrodes based on $NiCo_2S_4$, like $NiCo_2S_4$/functionalized multi-walled carbon nanotube (MWCNT) [52], $NiCo_2S_4$/N, S co-doped graphene [53], $NiCo_2S_4/MoS_2$ [54], etc. In a recent work, a microwave-assisted approach has been reported for the synthesis of the composite based on $NiCo_2S_4$ and reduced graphene oxide (RGO) [55]. In this process, initially, the graphite oxide solution was mixed with the ethylene glycol, nitrate salts of Co and Ni, and CS_2. In the next step, the solution was heated for 15 min at a temperature of 150 °C in a microwave reactor (1000 W) to form the composite. Compared to the conventional approaches, this microwave-assisted approach has the advantage of a shorter reaction time.

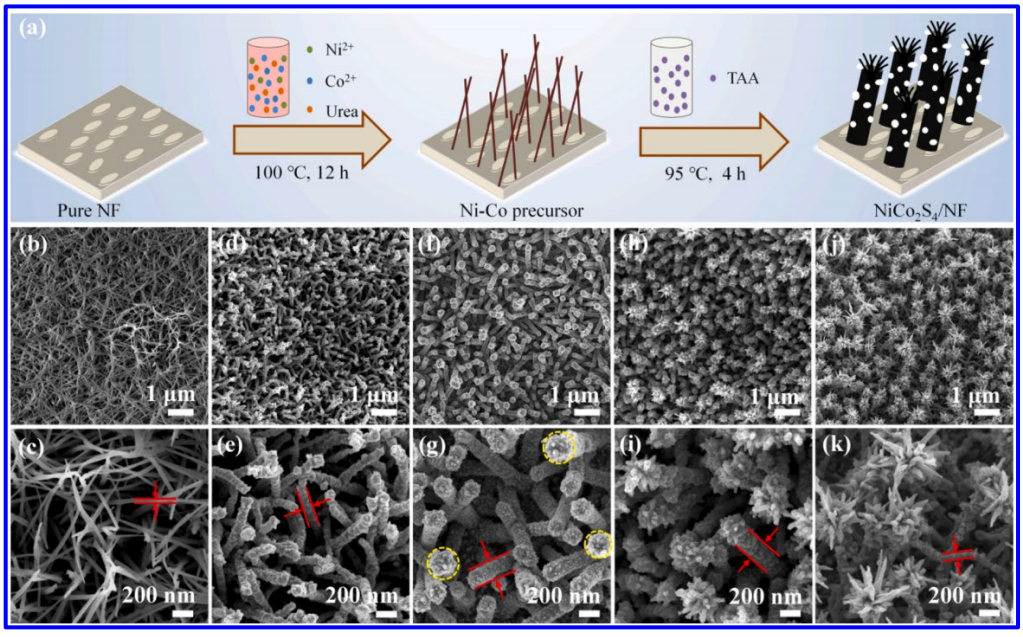


Figure 4. (**a**) Schematics of the hydrothermal synthesis of $NiCo_2S_4$ on NF; the SEM images of various $NiCo_2S_4$-coated NF after hydrothermal treatment of different time intervals: (**b**,**c**) Ni-Co precursor (after first hydrothermal treatment); (**d**,**e**) NiCoS-2 (after second hydrothermal reaction time of 2 h); (**f**,**g**) NiCoS-3 (after second hydrothermal reaction time of 3 h); (**h**,**i**) NiCoS-4 (after second hydrothermal reaction time of 4 h); (**j**,**k**) NiCoS-5 (after second hydrothermal reaction time of 5 h) [50].

Apart from the NF, the $NiCo_2S_4$ was also synthesized on other substrates. For example, Chen et al. demonstrated the formation of $NiCo_2S_4$ meshes through a two-step hydrothermal process and then combined them with $Ni(OH)_2$ through electrochemical deposition (Figure 5a) [56]. The unique combination of the 2D nanosheets ($NiCo_2S_4$) and 1D nanowires ($Ni(OH)_2$) has significant advantages for the fabrication of binder-free SC electrodes in terms of higher mass loading, easy electron and ion transport, and the prominent usage of interior active materials (Figure 5b). As a result, the electrode displayed higher areal capacity. The probable electrochemical reactions during the first hydrothermal process of forming the Ni-Co precursor on carbon cloths are provided below:

$$NH_4F \rightarrow NH_4^+ + F^- \quad (4)$$

$$Co(NH_2)_2 + H_2O \rightarrow 2NH_3 + CO_2 \quad (5)$$

$$NH_3 + H_2O \rightarrow NH_4^+ + OH^- \quad (6)$$

$$Ni^{2+} + 2Co^{2+} + 6OH^- \rightarrow NiCo_2(OH)_6 \quad (7)$$

$$CO_2 + H_2O \rightarrow CO_3^{2-} + 2H^+ \quad (8)$$

$$NiCo_2(OH)_6 + 1.5CO_3^{2-} + 0.1H_2O \rightarrow NiCo_2(CO_3)1.5(OH)_3 \cdot 0.11H_2O + 3OH^- \quad (9)$$

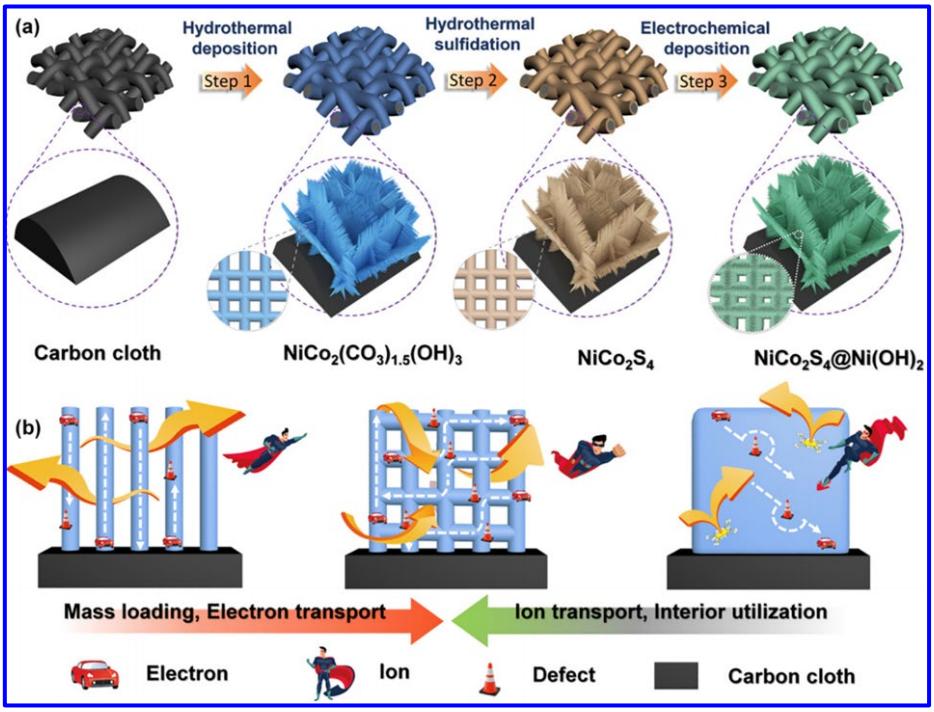


Figure 5. (**a**) Schematics of $NiCo_2S_4/Ni(OH)_2$ meshes on carbon cloth, and (**b**) the advantages of forming such a composite in the field of SC [56].

Apart from $NiCo_2S_4$, other NMS materials have also been synthesized through different synthetic approaches. Min et al. reported the two-step hydrothermal synthesis of the $FeNi_2$-LDH@$FeNi_2S_4$ core-shell nanocomposite [57]. In another work, a single-step solvothermal approach (ethylene glycol was used as the solvent) was reported for the Ni-Mn-S/RGO composite [58]. MOF-derived NMS materials have also been reported for SC applications. In this aspect, Cui et al. demonstrated the synthesis of RGO/Ni_2ZnS_4 composite using ZIF-8 through the Ni salt etching, high-temperature carbonization, and consequent hydrothermal vulcanization processes [59]. Furthermore, $NiZn_2O_4/NiZn_2S_4$ mesoporous nanocomposite was synthesized through a hydrothermal process on the NF

substrate [60]. Overall, it can be concluded that several NS and NMS materials and their related composites have been investigated as energy storage/conversion electrodes. However, most of the synthetic approaches are based on hydrothermal treatments.

4. Energy Storage and Conversion Application of NS and NMS Materials

4.1. Supercapacitor (SC)

NS and NMS materials have been extensively utilized for the fabrication of SC electrodes in the last few years. It is important to note that NS materials exist in different phases, including α-NiS, β-NiS, NiS_2, Ni_3S_4, Ni_7S_6, and Ni_3S_2. On the other hand, NS materials with diverse morphologies, including nanosheets, nanospheres, nanorods, etc., have been reported as the SC electrodes. For example, Yan et al. reported the evaluation of NiS nanosheets, grown on NF, as the SC electrode with a good specific capacitance (Csp) of 2587 F g^{-1} at a current density (CD) of 0.2 A g^{-1} [39]. Notably, the binder-less electrode further displayed a cycling stability (CS) of 95.8% after 4000 cycles. In order to demonstrate the practical utilization of the electrode, a hybrid SC device was also fabricated with an energy density (ED) of 38 Wh kg^{-1}. In another work, a ternary composite based on $NiS_{1.03}$, Ni_7S_6, and carbon exhibited the Csp of 1554.6 F g^{-1} [61]. Interestingly, the asymmetric device based on the ternary composite as the positive and the activated carbon as the negative electrode revealed relatively higher ED (41.2 Wh kg^{-1}) than the above-discussed NiS/NF-based device. Additionally, the device also demonstrated a good CS of 86.8% after 10,000 cycles. In another study, the integration of NiS with functionalized MWCNTs enhanced the Csp from 1400 to 1966 F/g at a current density (CD) of 1 A g^{-1} [62]. Notably, the rate capability also enhanced from 64% to 78%. Such a significant increment in performance was credited to the increment in electrochemically active sites with the addition of MWCNT to the NiS. On the other hand, the synergy between the pseudocapacitive NS and EDLC-type CNT also played a significant role in improving the performance. The corresponding asymmetric device NiS/MWCNT//AC also displayed higher ED (74.1 Wh kg^{-1}) than NiS//AC device (58 Wh kg^{-1}). In another work, a binder-free SC electrode based on CuCoSe and NiS was grown on NF with an ultrathin nanosheet morphology [63]. Due to its high surface area and enhanced electrochemically active sites, the electrode exhibited better performance than its primary counterparts, such as NiS/NF and CuCoSe/NF. As shown in Figure 6a,b, the composite electrode displayed higher current response in CV curves and superior charge–discharge time in GCD profiles than NiS/NF and CuCoSe/NF. The CV and GCD profiles of CuCoSe/NiS/NF composite electrode demonstrate the sign of pseudocapacitive nature (Figure 6c,d). On the other hand, the composite also displayed a superior rate performance than its other counterparts and higher Csp than the other related, reported electrode materials, indicating its promising application potential in SCs (Figure 6e,f). Apart from these, the composite also displayed lower solution resistance and charge transfer resistance, signifying a better conductive nature (Figure 6g). Furthermore, the electrode retained 98% of its initial Csp over 1000 charge/discharge cycles (Figure 6h). As schematically shown in Figure 6i, the transport of electrons and electrolyte ions is found to be easier for the composite electrode than its related counterparts. As a whole, the electrode revealed the Csp of 2937.5 F g^{-1}, and the corresponding SC device displayed a maximum ED of 41.8 Wh kg^{-1}. The uniform nanosheet structures of the electrode provided adequate channels for the transport of electrolyte ions and also improved the surface area, improving the supercapacitive performance.

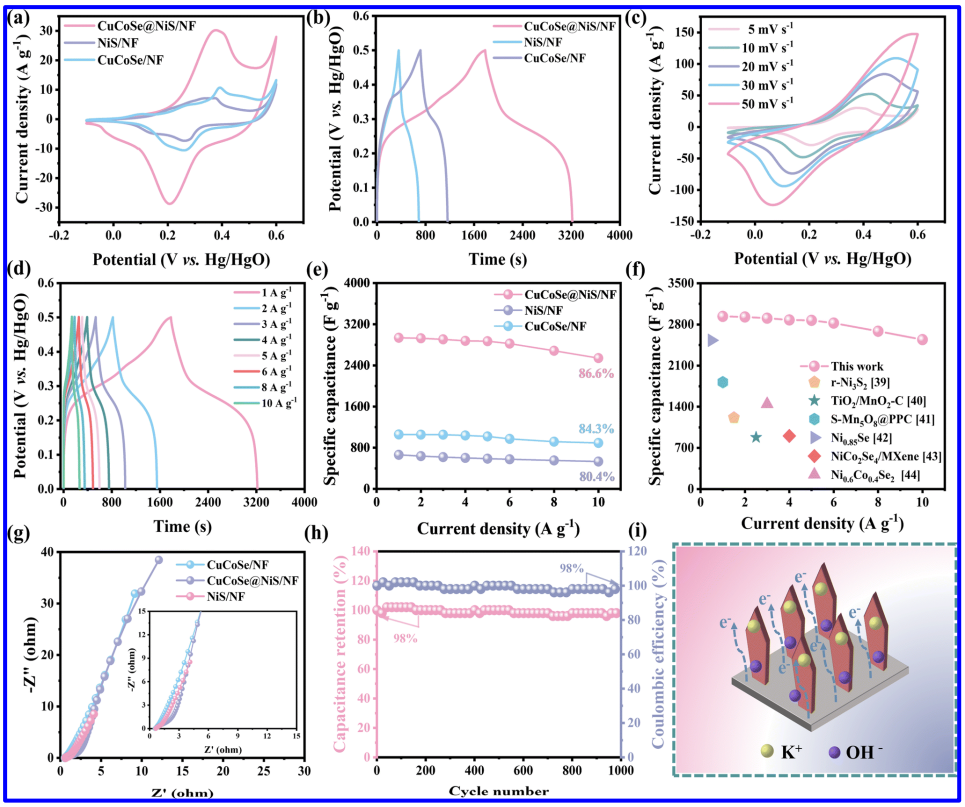


Figure 6. The SC performance of CuCoSe/NiS/NF composite and related electrode materials: (**a**) CV curves at 5 mV s^{-1}, (**b**) GCD profiles at 1 A g^{-1} of NiS/NF, CuCoSe/NF and CuCoSe/NiS/NF; (**c**) CV curves and (**d**) GCD profiles of CuCoSe@NiS/NF; (**e**) Csp at different CDs for all electrodes; (**f**) comparison of the Csp of CuCoSe/NiS/NF and some related, reported electrodes; (**g**) Nyquist plots of all electrodes; (**h**) the CS curve of CuCoSe/NiS/NF, measured at 15 A g^{-1}; (**i**) schematic representation of the electron and ion transport of CuCoSe/NiS/NF electrode during the charge–discharge process [63].

The NS materials have also been combined with EDLC-type 2D graphene materials. For example, Darsara et al. described the synthesis of NiS, Ni_3S_4, and RGO, which exhibited the Csp of 1578 F g^{-1} at the CD of 0.5 A g^{-1} in 2M KOH electrolyte [64]. The starfish-like 3D electrode also displayed a good CS of 91% after 5000 cycles. The electrochemical reactions of the NS materials during the charge–discharge process are shown below:

$$NiS + 3OH^- \leftrightarrow NiS(OH)_3 + 3e^- \quad (10)$$

$$Ni_3S_4 + OH^- \leftrightarrow Ni_3S_4OH + e^- \quad (11)$$

In another work, a hollow-structured composite electrode based on NiS_2, PANI, and graphene oxide was reported to display a specific capacity (Cs) of 536.13 C g^{-1} at a CD of 1 A g^{-1} [65]. Notably, a hybrid SC device was fabricated in this work, using the composite as the positive and AC as the negative electrode. The schematics of the device are shown in Figure 7a. As shown in Figure 7b,c, the device displayed its potential to be operated at a high operating potential of 1.6 V. The GCD profiles demonstrate the superior redox behavior of the device (Figure 7d). Additionally, the device exhibited a maximum ED of 13.09 Wh kg^{-1}, as observed from the Ragone plot in Figure 7e. Furthermore, the capacity retention of the device was found to be 86.59% over 10,000 charge/discharge cycles (Figure 7f).

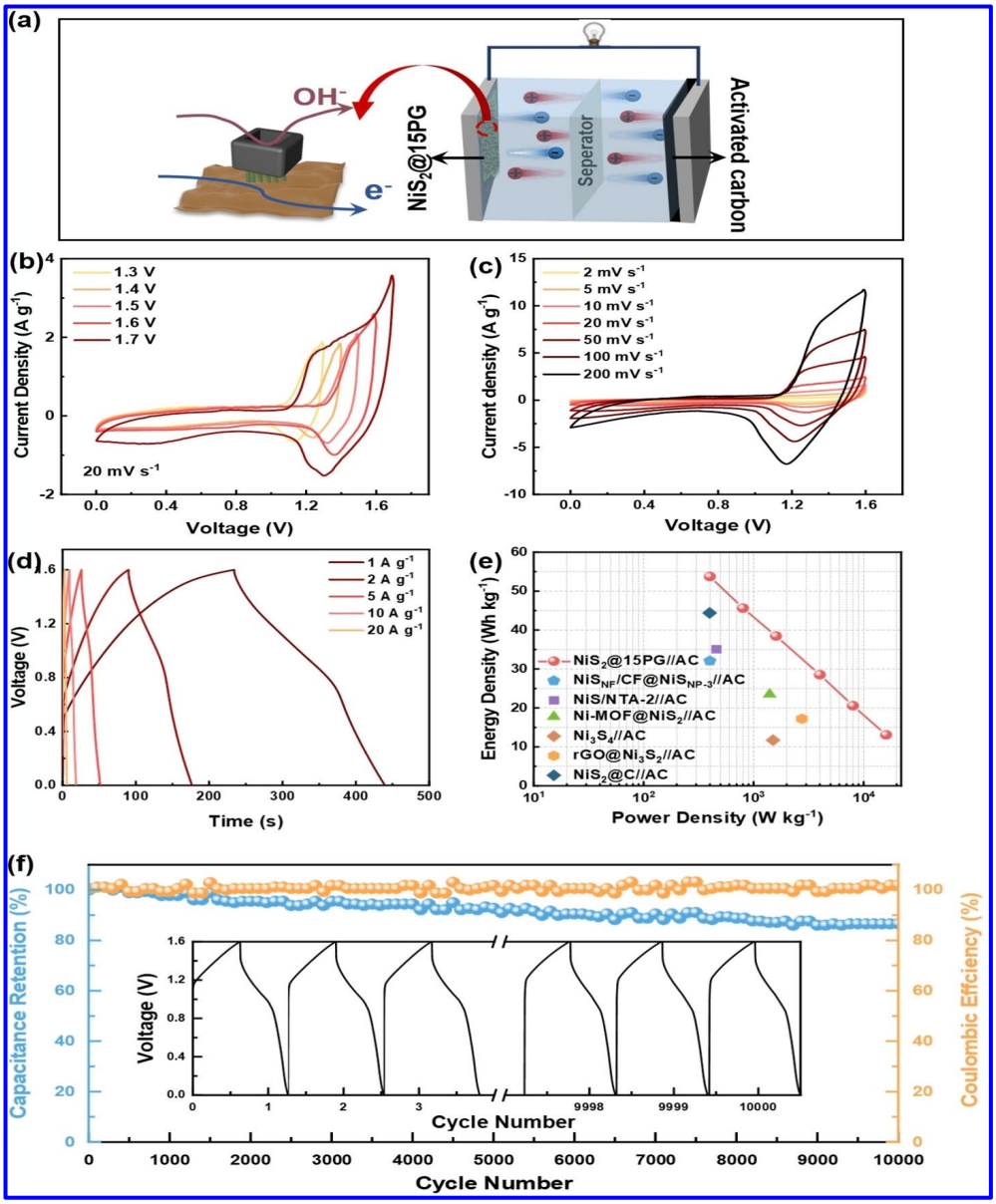


Figure 7. The electrochemical performance of NiS_2/PANI/graphene oxide composite (NiS_2@15PG)-based hybrid SC device: (**a**) Schematics of the device based on NiS_2@15PG as positive and AC as negative electrode, (**b**) CV profiles at different voltages (20 mV s^{-1}), ranging from 1.3 to 1.7 V, (**c**) CV curves at different scan rates (SRs), (**d**) GCD profiles at different CDs, (**e**) the Ragone plot, (**f**) the CS curve [65].

It is evident that the NiS displayed higher electrochemical performance than its oxide counterpart. In this aspect, a recent article is dedicated to a direct comparison of the supercapacitive performance of such materials [66]. At the current density of 5 A g^{-1}, NiS exhibited the Csp of 1066 F g^{-1}, which was higher than NiO (Csp of 166 F g^{-1}). The enhanced charge storage of the sulfide was attributed to its higher electrical conductivity, enhanced pseudocapacitive behavior, larger surface area, enhanced redox kinetics, and strong interaction with the electrolyte (3 M KOH).

Among the NMS materials, $NiCo_2S_4$ is the most-studied one because of its easy synthetic approaches, high chemical stability, and enhanced redox characteristics. Chen et al. revealed the fabrication of a flexible SC electrode by integrating $NiCo_2S_4$ with $Ni(OH)_2$ [56]. The mesh-like electrode displayed an areal capacity of 246.9 mAh g^{-1}. Additionally, the solid-state asymmetric SC (ASC) device exhibited the ED of 315 µWh cm^{-2} at the corre-

sponding power density of 2.14 mW cm^{-2}. Additionally, the operating voltage of the device has been enhanced to 5V by connecting three devices in series. Furthermore, the current response could be improved by connecting three devices in parallel, as demonstrated in Figure 8a,b. Negligible loss of capacity has been monitored at various bending angles of the device, indicating its promising flexibility (Figure 8c). The practical utility of the devices was further confirmed by glowing red and green LEDs after charging the device for a definite time interval (Figure 8d,e). Notably, the advanced SC device in connection with another unit was able to power a headphone and an electronic watch, enabling its significant potential for future electronics (Figure 8f). In another work, the hydrothermally synthesized Ni_2ZnS_4/RGO composite exhibited the Csp of 1150 F g^{-1} at the CD of 1 A g^{-1} [59]. However, the CS of the composite was found to be poor (capacitance retention of 59.7% after 2000 cycles), which can be attributed to the structural breakdown during the repeated charge/discharge process. The Csp was further enhanced by combining RGO with Ni-Mn-S. The solvothermally synthesized composite electrode displayed a superior Csp of 2042.22 F g^{-1} at the CD of 1 A g^{-1} [58]. Compared to the previously discussed Ni_2ZnS_4/RGO composite, the electrode also demonstrated better CS of 77.78% over 5000 cycles. Additionally, the SC device based on the composite electrode as the positive and AC as the negative electrode retained 81.97% of its initial capacitance over 10,000 charge–discharge cycles. In another work, the hydrothermally synthesized $Ni_{1-x}Cu_xS$ displayed a maximum Csp of 1092 F g^{-1}, which was found to be higher than its single metal sulfide counterparts like NiS (575 F g^{-1}) and Cu_9S_5 (70 F g^{-1}) [67]. This study signifies the importance of MNS materials in the field of energy storage. Alitabar et al. reported the hydrothermal growth of Ni-Co-Fe-S nanosheets on NF, which exhibited the Cs of 1156 C g^{-1} and the rate capability of 81.1% [68]. The enhanced electrochemical performance of the battery-type SC electrode was ascribed to its high surface area (84.3 m^2 g^{-1}) and enhanced porosity. The superior redox activity was identified from the noticeable redox peaks in CV curves at different SRs, which can be assigned to the following redox reactions.

$$Ni_3S_2 + 3OH^- \leftrightarrow Ni_3S_2(OH)_3 + 3e^- \quad (12)$$

$$FeS_2 + OH^- \leftrightarrow FeS_2OH + e^- \quad (13)$$

$$CoS_2 + OH^- \leftrightarrow CoS_2OH + H_2O + e^- \quad (14)$$

$$CoS_2OH + OH^- \leftrightarrow CoS_2O + H_2O + e^- \quad (15)$$

In another work, a core-shell structured composite electrode based on $FeNi_2$-LDH and $FeNi_2S_4$ was reported to deliver a Cs of 450 C g^{-1} at a high CD of 6 A g^{-1} [57]. Notably, the electrode displayed a good CS of 92.3% over 5000 cycles due to its enhanced structural stability and higher porosity. Table 1 represents a comparative study on the electrochemical performance of a few NS and MNS materials. The electrochemical performance of these electrodes was reported to be measured in aqueous KOH electrolyte. However, the concentration of the electrolyte varies in different works. As shown in the table, the sulfide-based electrodes have been combined with other metal sulfides, oxides, carbon materials, LDH, etc. The electrode demonstrated good charge storage performance in terms of superior capacitance/capacity and CS over longer charge/discharge cycles. Jinlong et al. compared the electrochemical performance of NF-grown $NiCo_2O_4$ and $NiCo_2S_4$ [69]. The NMS material exhibited a higher surface area (75.8 m^2 g^{-1}) than its oxide counterpart (41.84 m^2 g^{-1}). Accordingly, the mixed sulfide also displayed better cycling stability (92.1%) than the mixed oxide (84.8%) over 5000 charge–discharge cycles.

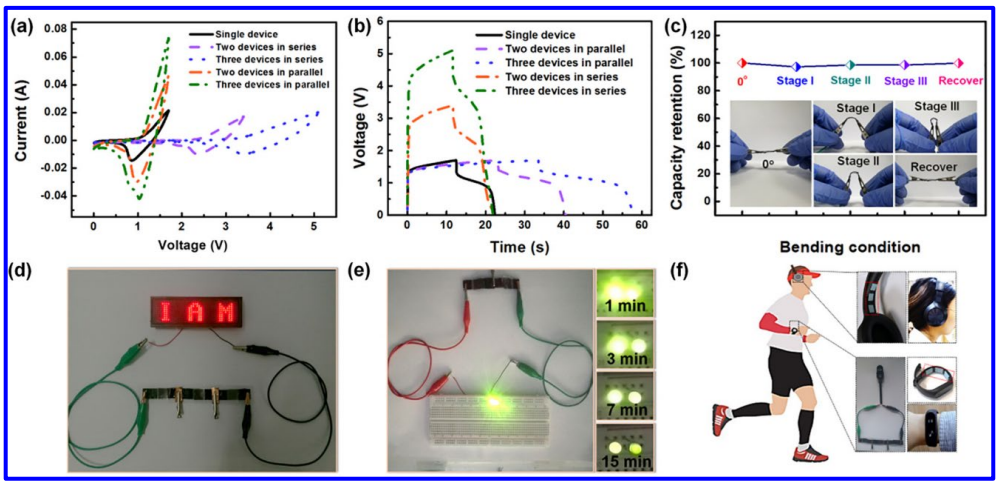


Figure 8. The electrochemical performance of the flexible $NiCo_2S_4/Ni(OH)_2//Fe_2O_3$ device: the (**a**) CV and (**b**) GCD curves of the devices connected in series or in parallel at SR of 20 mV s^{-1} and CD of 50 mA cm^{-2}, respectively; (**c**) the plot of capacity retention of the device at different bending angles, demonstrating superior flexibility, (**d**) the digital images of three flexible devices, connected in series, lighting red LED display, (**e**) the image of the glow up of yellow LED with the series connection of two flexible devices, and (**f**) the image of three in series connection for functioning a headphone and an electronic watch [56].

Table 1. Comparison of the electrochemical performance of a few NS and NMS materials for SC applications.

Electrode	Electrolyte (Conc. of KOH)	Specific Capacitance (F g^{-1}) or Specific Capacity (C g^{-1})	Cycling Stability (%)	Ref.
β-NiS	2 M	638.34 C g^{-1} at 1 A g^{-1}	-	[40]
NiS/NF	3 M	2587 F g^{-1} at 0.2 A g^{-1}	95.8 after 4000 cycles	[39]
α-NiS/β-NiS	3 M	2250 F g^{-1} at 2 mV s^{-1}	-	[47]
$NiS_{1.03}/Ni_7S_6$/Carbon	6 M	1554.6 F g^{-1} at 1 A g^{-1}	80.4 after 5000 cycles	[61]
NiS/functionalized-MWCNT	6 M	1966 F g^{-1} at 1 A g^{-1}	86.2 after 10,000 cycles	[62]
Co_3O_4/NiS/NF	6 M	1395.3 F g^{-1} at 1 A g^{-1}	89.9 after 5000 cycles	[70]
CuCoSe/NiS/NF	3 M	2937.6 F g^{-1} at 1 A g^{-1}	98 after 1000 cycles	[63]
Ni_3S_4/NiS/RGO	2 M	1578 F g^{-1} at 0.5 A g^{-1}	91 after 5000 cycles	[64]
NiS_2/PANI/graphene	1 M	536.13 C g^{-1} at 1 A g^{-1}	80.5 after 5000 cycles	[65]
P-doped Co_3S_4/Ni_3S_4/NF	2 M	3614 F g^{-1} at 1 A g^{-1}	73 after 3000 cycles	[43]
$Ni_3S_2/CoMoS_4/MnO_2$/NF	1 M	2021 F g^{-1} at 1 A g^{-1}	90 after 4000 cycles	[71]
$Mg(OH)_2/Ni_3S_4$	1 M	3316.7 F g^{-1} at 1 A g^{-1}	-	[49]
Cu2S/NiS/Ni_3S_4	6 M	363.05 mAh g^{-1} at 0.5 A g^{-1}	94.8 after 8000 cycles	[42]
$Co_9S_8/NiS_2/Cu_2S$/NF	3 M	460.15 C g^{-1} at 1 A g^{-1}	-	[48]
$NiCo_2S_4$	3 M	3506 F g^{-1} at 2 A g^{-1}	90 after 5000 cycles	[51]
$NiCo_2S_4$/functionalized MWCNT	6 M	1360 F g^{-1} at 1 A g^{-1}	80.6 after 10,000 cycles	[52]
$NiCo_2S_4/MoS_2$	3 M	2594 F g^{-1} at 0.8 A g^{-1}	192 after 45,000 cycles	[54]
$NiCo_2S_4/SnS_2$	1 M	329.22 mAh g^{-1} at 2 A g^{-1}	76.87 after 10,000 cycles	[72]

Table 1. *Cont.*

Electrode	Electrolyte (Conc. of KOH)	Specific Capacitance (F g^{-1}) or Specific Capacity (C g^{-1})	Cycling Stability (%)	Ref.
$NiCo_2S_4$/CoAl-LDH	3 M	2120 F g^{-1} at 1 A g^{-1}	98.96 after 10,000 cycles	[73]
$NiCo_2S_4$/Mo-doped Co-LDH/carbon cloth	3 M	3049.3 F g^{-1} at 1 A g^{-1}	91 after 10,000 cycles	[74]
$FeNi_2$-LDH/$FeNi_2S_4$	1 M	806 C g^{-1} at 1 A g^{-1}	92.3 after 5000 cycles	[57]
Ni-Co-Mn-S	6 M	661 C g^{-1} at 1 A g^{-1}	-	[75]
Zn-Ni-Co-S/Zn-Ni-Co-O	6 M	1445 C g^{-1} at 1 A g^{-1}	86.1 after 3000 cycles	[76]
$NiZn_2O_4$/$NiZn_2S_4$/NF	1 M	1516 C g^{-1} at 1 A g^{-1}	86.9 after 10,000 cycles	[60]
$Ni_{1.43}Fe_{0.5}Co_{0.5}S_{0.97}$/NF	6 M	1156 C g^{-1} at 2 A g^{-1}	92.9 after 10,000 cycles	[68]
Ni_2ZnS_4/RGO	6 M	1150 F g^{-1} at 1 A g^{-1}	59.7 after 2000 cycles	[59]
Ni-Mn-S/RGO	2 M	2042.22 F g^{-1} at 1 A g^{-1}	77.78 after 5000 cycles	[58]

Overall, the enhanced charge storage of the Ni-based electrodes is ascribed to their improved redox activity, enhanced porosity, and high surface area. Benefited by such characteristics, Ni-based materials have also been employed for energy conversion applications. The next section is dedicated to exploring the energy conversion (OER) applications of such materials.

4.2. OER

Among the various transition metal sulfides/mixed sulfides, NS and NMS have emerged as one of the most effective electrocatalysts for water splitting, particularly for the oxygen evolution reaction (OER). Specifically, NS's exceptional performance is attributed to several factors: it exists in multiple crystalline phases (such as NiS, NiS_2, and Ni_3S_2), many of which exhibit low OPs, enhancing catalytic efficiency; it shows excellent electrochemical stability in alkaline media, which is essential for long-term durability; and its polymorphic forms and ability to form heterostructures contribute to a high density of active sites, thereby improving catalytic activity. Furthermore, nickel is significantly more abundant and cost-effective compared to precious metals like platinum, ruthenium, and iridium, making nickel sulfide a practical and scalable alternative for OER through electrochemical water splitting. An excellent electrocatalyst for OER should possess key characteristics such as low OP, fast reaction kinetics, a large electrochemically active surface area (ECSA), low charge transfer resistance (Rct), and high long-term stability. Recently, various synthesis methods have been employed to optimize these parameters in NS materials, aiming to significantly enhance their OER performance. For instance, Ni et al. employed a straightforward solid-state synthesis method to fabricate transition-metal sulfide heterostructures, specifically MoS_2/NiS_2 and WS_2/NiS_2 [77]. These heterostructures exhibited significantly improved OER performance, with low OPs of 300 mV for MoS_2/NiS_2 and 320 mV for WS_2/NiS_2 at a CD of 10 mA cm^{-2}. Additionally, they achieved smaller Tafel slopes of 60 mV dec^{-1} and 83 mV dec^{-1}, respectively, in 1 M KOH solution. These results not only surpass the performance of their individual components, MoS_2, WS_2, and NiS_2, but also outperform the benchmark RuO_2 catalyst, highlighting the potential of heterostructure engineering as a powerful strategy for advancing NS-based electrocatalysts (Figure 9a–c) [77].

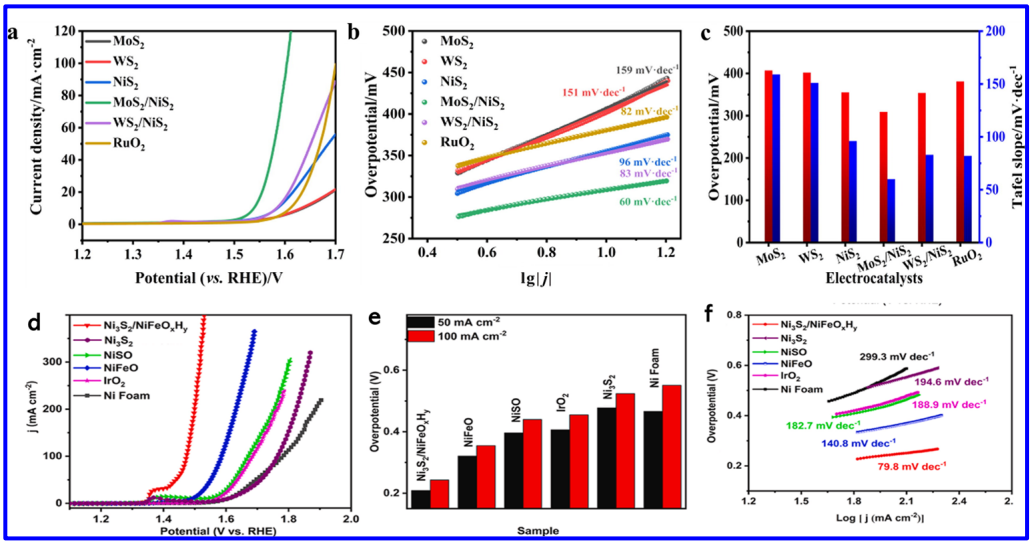


Figure 9. OER activity of various NS materials: (**a**) LSV curves, (**b**) Tafel slopes, and (**c**) comparison of OPs at 10 mA cm^{-2} and Tafel slope for MoS_2, WS_2, NiS_2, MoS_2/NiS_2, WS_2/NiS_2, and RuO_2 2 [77]; (**d**) OER LSV curves, (**e**) OPs at 50 and 100 mA cm^{-1}, and (**f**) Tafel plots for NF, IrO_2, NiSO, NiFeO, Ni_3S_2, and $Ni_3S_2/NiFeO_xH_y$ [78].

In another work, Zhou et al. synthesized a Ni_3S_2/NiFe-(oxy) hydroxide ($NiFeO_xH_y$) heterostructure nanosheet array that exhibited outstanding OER performance with ultralow OPs of 209 mV and 243 mV to achieve the current densities (CDs) of 50 and 100 mA cm^{-2}, respectively (Figure 9d–f). These values are found to be lower than those of Ni_3S_2 (480 mV and 534 mV), NiSO (397 mV and 440 mV), NiFeO (321 mV and 355 mV), commercial IrO_2 (406 mV and 455 mV), and NF (466 mV and 551 mV), demonstrating superior catalytic activity. Notably, $Ni_3S_2/NiFeO_xH_y$ outperformed even the commercial IrO_2 catalyst. The Tafel slope of $Ni_3S_2/NiFeO_xH_y$ was 79.8 mV dec^{-1} at high CD (~100 mA cm^{-2}), which is much smaller than those of Ni_3S_2 (194.6 mV dec^{-1}), NiSO (182.7 mV dec^{-1}), NiFeO (140.8 mV dec^{-1}), IrO_2 (188.9 mV dec^{-1}), and NF (299.3 mV dec^{-1}), indicating faster OER kinetics (Figure 9f). This remarkable activity arose from the synergistic coupling between Ni_3S_2 and $NiFeO_xH_y$ phases, which enhanced charge transfer, increased the density of active sites, and improved overall stability [78]. On the other hand, Shi et al. synthesized molybdenum-doped Ni_3S_4 nanosheets grown on carbonized wood (Mo-Ni_3S_4/CW) [79]. The synthetic approach is schematically shown in Figure 10a. The theoretical calculations revealed that Mo-doping caused lattice expansion in Ni_3S_4, which optimized the adsorption energies of hydrogen and oxygen species. This adjustment regulated the local charge density at active sites, thereby enhancing the OER activity (Figure 10b). The Mo-Ni_3S_4/CW-0.4 catalyst exhibited OPs of 240 mV and 337 mV to reach CDs of 10 and 100 mA cm^{-2}, respectively, outstripping undoped Ni_3S_4/CW (η_{10} = 343 mV) (Figure 10c). Moreover, Mo-Ni_3S_4/CW-0.4 showed the lowest Tafel slope of 47.7 mV dec^{-1}, indicating superior OER kinetics compared to Ni_3S_4/CW (115.7 mV dec^{-1}) and even commercial RuO_2 (66.6 mV dec^{-1}) (Figure 10d).

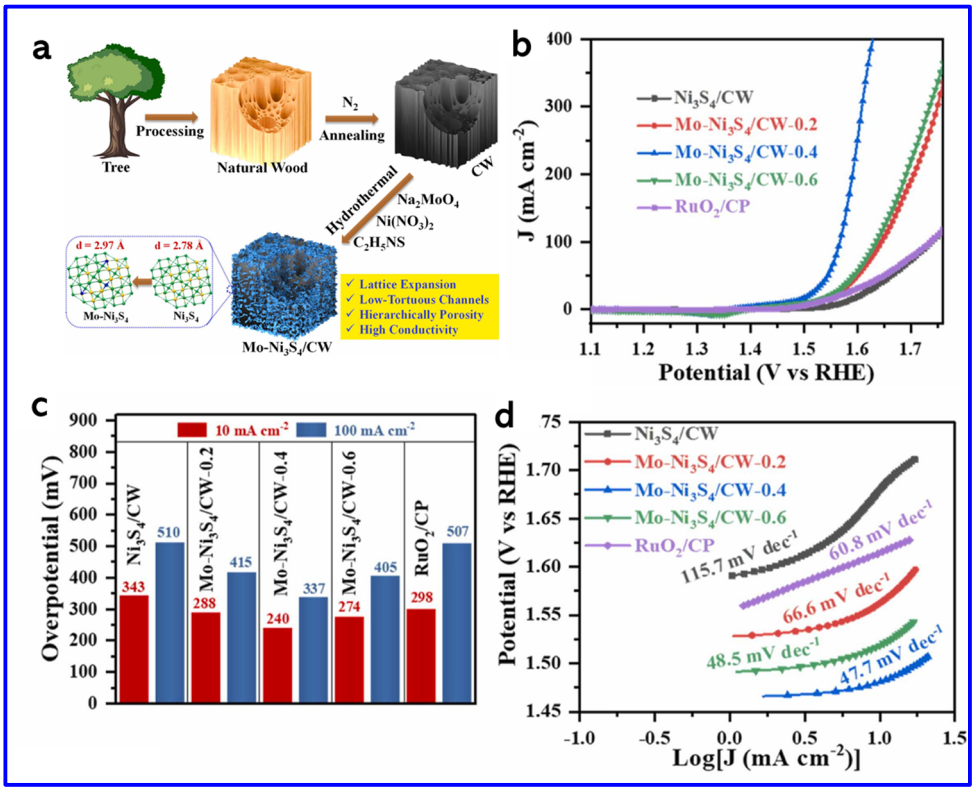


Figure 10. (**a**) Schematics of the synthesis of Mo-Ni_3S_4/CW, (**b**) the LSV curves, (**c**) corresponding OP histograms at 10 and 100 mA cm^{-2}, and (**d**) Tafel plots [79].

Metal-doping is another strategy for enhancing the catalytic activity of NS materials. In this context, Prakash et al. synthesized Zn-doped NiS nanosheets on NF using a simple hydrothermal method [80]. The optimized sample, Zn-NiS-3, exhibited the best OER performance, achieving an OP of 320 mV at a CD of 50 mA cm^{-2}, which is significantly lower than that of undoped NiS. The enhanced catalytic activity is attributed to the incorporation of Zn, which likely improves the electronic structure and promotes charge transfer during the oxygen evolution reaction. In another work, Wang et al. developed a dual-doped NS catalyst (Fe/W-Ni_3S_2) grown on NF, exhibiting significantly enhanced OER performance [81]. The hydrothermal-assisted ion-exchange process was adopted to grow the doped NS material on NF, as shown in Figure 11a. The improved activity is attributed to the synergistic effect between iron doping and nickel vacancies introduced by tungsten leaching during the in situ oxidation process. This combination maximizes the exposure of active OER sites and enhances charge transport, thereby accelerating the reaction kinetics (Figure 11b). The Fe/W-Ni_3S_2 catalyst achieved low OPs of 222 mV and 261 mV at CDs of 10 and 100 mA cm^{-2}, respectively, outperforming Fe-Ni_3S_2 (229 and 298 mV), W-Ni_3S_2 (284 and 358 mV), and undoped Ni_3S_2 (350 and 479 mV) (Figure 11c). It also exhibited the lowest Tafel slope of 38 mV dec^{-1}, compared to 52, 61, and 178 mV dec^{-1} for Fe-Ni_3S_2, W-Ni_3S_2, and Ni_3S_2, respectively, confirming its enhanced OER kinetics (Figure 11d). These findings demonstrate that dual doping is an effective strategy for boosting the catalytic performance of NS materials.

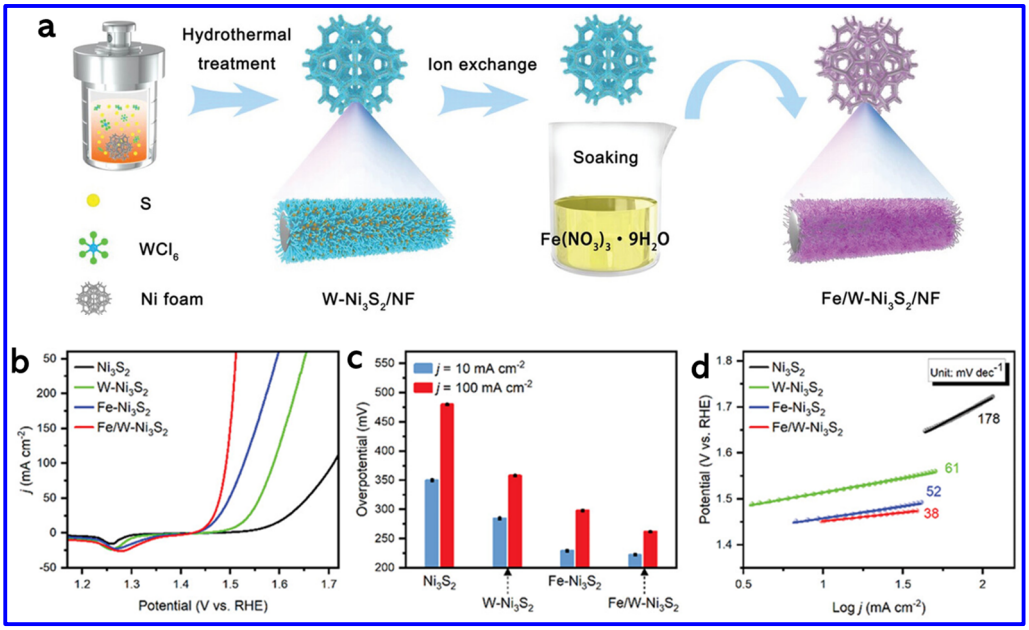


Figure 11. (**a**) Schematics of the synthesis process of Fe/W-Ni_3S_2, (**b**) LSV curves for OER of Ni_3S_2, W-Ni_3S_2, Fe-Ni_3S_2, and Fe/W-Ni_3S_2 (with 85% iR-compensation). (**c**) OPs at different CDs. (**d**) Corresponding Tafel slopes [81].

A recent work reported the synthesis of Cu and Co co-doped Ni_3S_2 catalyst (CuCo-Ni_3S_2/NF) on NF using a hydrothermal method followed by liquid-phase vulcanization [82]. The optimized catalyst, with a 1:1 molar ratio of copper to cobalt, exhibited higher OER performance, achieving a low OP of 400 mV at a CD of 100 mA cm^{-2}. This outperforms Co-Ni_3S_2/NF (425 mV), Cu-Ni_3S_2/NF (430 mV), Ni_3S_2/NF (438 mV), and even RuO_2/NF (460 mV) under the same conditions. The improved catalytic activity is attributed to the synergistic effects among the three transition metals. Specifically, Co-doping increased the number of exposed active sites, while Cu incorporation enhanced the charge transfer rate. Together, these factors contributed to the superior electrocatalytic performance of CuCo-Ni_3S_2/NF. Furthermore, Mao et al. prepared Fe and Co dual-doped Ni_3S_4 nanosheets using a two-step hydrothermal method [83]. The dual-doped catalyst demonstrated excellent OER performance, with OPs of 230 mV and 280 mV at CDs of 10 and 100 mA cm^{-2}, respectively. These values are significantly lower than those for Fe-Ni_3S_4 (257 and 307 mV), Co-Ni_3S_4 (260 and 317 mV), pure Ni_3S_4 (268 and 357 mV), and the precursor nanosheets (238 and 310 mV). The improved performance is attributed to a combination of high Ni^{3+} content that enhances OH^- adsorption and electron transfer, strong adhesion to the NF substrate for improved conductivity and stability, and synergistic effects from dual cation doping. Additionally, oxygen doping or surface hydroxides formed during OER may further boost catalytic activity.

The morphology and crystal phase have a significant impact on the OER efficiency of NS materials. In this aspect, Manjunatha et al. synthesized various polymorphs of nickel sulfide via a hydrothermal method and investigated, for the first time, the influence of morphology and crystalline structure on OER performance [84]. The catalytic activity followed the order: NiS > NiS_2 > Ni_3S_4. Among the different morphologies, NiS (sugar-cube-shaped) demonstrated the best performance, followed by NiS (agglomerated stone particles) and NiS (apple-shaped). For NiS_2, the order was: aggregated stone particles > rose-type > tubular bacteria-shaped. Notably, NiS (sugar cubes) achieved an OPof 362 mV at 20 mA cm^{-2}, outperforming even the benchmark RuO_2, which showed an OPof 416 mV under the same conditions. In another work, the NiS/rGO nanocomposite demonstrated

a markedly higher CD (1367 mA cm^{-2}) compared to pure NiS (536 mA cm^{-2}) and rGO (115 mA cm^{-2}), owing to the strong chemical interaction between nickel sulfide and the rGO nanosheets [85]. Additionally, the nanocomposite exhibited a lower onset potential of 1.40 V, indicating a reduced energy barrier for initiating the OER activity. According to the Tafel plots, the NiS/rGO composite showed the smallest Tafel slope (32 mV dec^{-1}), outperforming both NiS (52 mV dec^{-1}) and rGO (46 mV/dec), further revealing OPs of 216 mV for NiS, 369 mV for rGO, and only 162 mV for the composite at 10 mA cm^{-2}. The hetero-atom doping of carbon materials, in combination with NS materials, displayed better catalytic activity than their undoped counterparts. In a recent work, it has been observed that the N-doped graphene-like carbon layers/Ni_3S_2 composite, grown on NF, exhibited better OER activity compared to graphene-like carbon nanosheets/Ni_3S_2 composite [86]. This enhanced performance is attributed to the unique heterogeneous architecture formed by N-doped CNT and Ni_3S_2 nanowires, which synergistically improved catalytic efficiency. In another work, the NiS/NiO/N-doped CNT, grown on NF, demonstrated superior OER performance, achieving a notably low OPof 269 mV at 10 mA cm^{-2} [87]. This value is significantly lower than those recorded for NiO/N-doped CNT/NFs (390 mV), Ni/N-doped CNT/NF (470 mV), and commercial RuO_2 (347 mV). The Tafel slope analysis further confirmed the enhanced kinetics, with NiS/NiO/N-doped CNT/NFs showing a much smaller slope of 48.4 mV dec^{-1} compared to 221.4, 140.5, and 67.1 mV dec^{-1} for NiO/N-doped CNT/NFs, Ni/N-doped CNT/NFs, and RuO_2, respectively. These findings suggest that the formation of NiS/NiO heterostructures significantly boosts both catalytic efficiency and reaction kinetics in OER. NMS materials have also been combined with other advanced functional materials for the fabrication of electrocatalysts for OER applications. In this aspect, Yang et al. reported the fabrication of an OER catalyst based on 3D heterostructures by adhering needle-like $NiCo_2S_4$ particles on NiCo alloys embedded N-doped carbon fibers [88]. Owing to the synergistic contribution from the alloy and the semiconductor-type carbon fibers, the heterostructured composite achieved a low OP of 291 mV at the CD of 10 mA cm^{-2}. Even at a higher CD of 100 mA cm^{-2}, the composite electrode exhibited an OP of 376 mV. In another work, the addition of Au significantly improved the catalytic activity of $NiCo_2S_4$ [89]. Compared to the base NMS materials, the composite electrode (312 mV) displayed a lower OP of 299 mV. Notably, the Tafel slope has also been reduced in the composite (44.5 mV dec^{-1}), in comparison with the bare NMS material (49.1 mV dec^{-1}). The NMS material was further combined with carbon materials. For instance, a recent work demonstrated the catalytic activity of a composite based on $NiCo_2S_4$ and S-doped g-C_3N_4 [90]. Benefitting from the high surface area and strong synergy between the individual components, the composite demonstrated a lower OP of 370 mV. It is important to note that the stability of NMS materials depends on several factors, including the stoichiometry, composition, chemical structure, and electrolyte, as well as surface transformation during OER activity. In some cases, the actual active species for OER could be the oxidation product of Ni-based sulfides, like Ni-based (oxy)hydroxides, formed through the surface transformation under OER conditions.

Apart from the $NiCo_2S_4$, other NMS materials have also been reported for enhanced OER activities. In this aspect, Ke et al. reported the fabrication of MOF-derived chalcogenide electrocatalysts based on $Fe_{0.75}Ni_{0.25}S_2$ and FeNiOOH [91]. The composite exhibited a lower OP of 247 mV, along with a smaller Tafel slope of 47.6 mV dec^{-1}. In another work, the electrocatalyst based on $Ni_{1.29}Co_{1.49}Mn_{0.22}S_4$ displayed good OER activity with a low OP of 348 mV at the CD of 10 mA cm^{-2} [92]. The catalyst also exhibited good activity towards the oxygen reduction reaction, indicating its potential applicability in Zn-air batteries. The enhanced catalytic performance was attributed to the high surface area, favorable electronic structure, and strong synergy between the various metal dopant species. Yang

et al. reported the formation of the heterostructures of Ni_3S_2 and $FeNi_2S_4$ on NF. The Ni form grown electrocatalyst exhibited an OP of 235 mV at the CD of 10 mA cm^{-2} [93]. In another work, the NF-grown Ni_3S_2/Co_3S_4 nanosheets demonstrated promising OER activity in alkaline seawater [94]. Such a seawater electrocatalysis process was found to be stabilized at higher current density up to 800 mA cm^{-2}. Furthermore, powered by a solar cell, the integrated device exhibited advanced seawater splitting with a high solar-to-hydrogen efficiency of 15.13%. These studies clearly demonstrate the promising electrocatalytic activities of NS and NMS materials. A comparative study on the OER activity of a few NS and NMS materials is summarized in Table 2. As shown in Table 2, the electrocatalysts exhibited lower OP and Tafel slope.

Table 2. Comparison of the electrochemical performance of a few NS and NMS materials for OER applications.

Sl. N.	Materials	Overpotential (mV) at 10 mA cm^{-2}	Tafel Slope (mV dec^{-1})	Ref.
1.	$NiCo_2S_4$/Carbon Nitrogen nanosheets	360	76	[95]
2.	Zn-doped NiS	320 (at 50 mA cm^{-2})	36	[80]
3.	$Ni_{1.5}Co_{1.5}S_4$	360	61	[96]
4.	$Ni_{1.29}Co_{1.49}Mn_{0.22}S_4$	348	65	[92]
5.	NiS	362 (at 20 mA cm^{-2})	65	[84]
6.	Co-Ni_3S_2/NF	274	199	[97]
7.	Fe/W-doped Ni_3S_2	222	38	[81]
8.	$Fe_{0.75}Ni_{0.25}S_2$/FeNiOOH	247	47.6	[91]
9.	CuNiS	337	43	[98]
10.	NiS	210	60	[99]
11.	Ni_3S_2/CoS_x	226	56	[100]
12.	NiS/rGO	162	32	[85]
13.	$Ni_3S_2/FeNi_2S_4$/NF	235	92	[93]
14.	FeCO/Ni_3S_4	230 (at 20 mA cm^{-2})	63.2	[83]
15.	V-doped Ni_3S_2/NF	268	99	[101]
16.	N-doped CNTs/NiS_2	235	88	[102]
17.	Mo-Ni_3S_4/Carbonized wood	240	47.7	[79]
18.	P-doped Ni_3S_2/NiS/NF	178	37	[103]
19.	Co-doped Ni_3S_2/NF	297 (at 20 mA cm^{-2})	50.3	[104]
20.	$NiCo_2S_4$/NiCo alloys/N-doped carbon fibers	291	51.17	[88]
21.	Au/$NiCo_2S_4$	299	44.5	[89]
22.	$NiCo_2S_4$/S-doped g-C_3N_4	370	99.2	[90]

5. Conclusions and Future Prospects

Ni-based chalcogenides have been efficiently integrated with other functional materials for high-performance energy storage and conversion applications in the last few years. Their enhanced characteristics, like high surface area, enhanced porosity, easy synthetic approaches, rich redox activity, and high abundance, permitted them to serve as effective electrode materials for SC and OER applications. Recent advancements of these materials and their electrochemical applications are systematically summarized in this review. Despite several advantages, a few drawbacks of these materials hamper their effective utilization in the field of energy storage and conversion. The existing challenges and the probable solutions are briefly summarized below:

1. The detailed charge storage mechanism of NMS materials has not been clearly explored yet. In this aspect, the suitable integration of theoretical calculations and experimental results is highly essential.
2. The subsequent volume expansion and the fallout of the active SC electrode materials from the current collectors negatively affect the cycling performance and rate capability. To solve this issue, specifically designed electrode materials with high chemical stability are essential.
3. All the relevant works reported the evaluation of the electrochemical performance of NS and NMS materials in KOH electrolyte. Further increment of electrochemical performance is possible through the addition of redox species in the electrolyte. However, in those cases, the cycling performance of the electrodes should be monitored carefully.
4. The charge storage kinetics should also be evaluated thoroughly. In the case of OER activity, the NMS materials have the tendency to oxidize easily to their oxide and hydroxide counterparts, which sometimes harms the OER activities by deteriorating stability and catalytic activity. To solve this issue, the NMS materials have been combined with metal oxides and hydroxides and sometimes grown on conductive substrates. However, in those cases, the catalyst loading should be provided with accuracy.
5. The in situ characterization techniques should be implemented to understand several factors, like the charge storage mechanism, the sources of enhanced catalytic activity, the interaction between the electrode and electrolytes, intermolecular interactions, and structural changes of the electrode during the repetitive electrochemical processes.

Witnessing the rapid progress in such materials in various fields, it is expected that the existing issues with the energy storage and conversion applications of NS and NMS materials will be systematically solved in the upcoming years.

Author Contributions: Conceptualization, G.D. and S.S.; methodology, G.D. and S.S.; formal analysis, G.D. and S.S.; investigation, G.D. and S.S.; resources, G.-L.Z.; writing—original draft preparation, G.D., K.P.S. and S.S.; writing—review and editing, S.S. and G.-L.Z.; visualization, G.D. and S.S.; supervision, G.-L.Z.; project administration, G.-L.Z.; funding acquisition, G.-L.Z. All authors have read and agreed to the published version of the manuscript.

Funding: This research received no external funding.

Institutional Review Board Statement: Not applicable.

Informed Consent Statement: Not applicable.

Data Availability Statement: No new data were created.

Acknowledgments: The study was supported by the US Army Research Office (ARO) (Award No. W911NF2210099) and the US National Science Foundation (NSF) (Award No. 2216805).

Conflicts of Interest: The authors declare no conflicts of interest.

References

1. Pershaanaa, M.; Bashir, S.; Ramesh, S.; Ramesh, K. Every bite of Supercap: A brief review on construction and enhancement of supercapacitor. *J. Energy Storage* **2022**, *50*, 104599. [CrossRef]
2. Kumar, R.; Sahoo, S.; Pandey, R.; Joanni, E.; Yadav, R.M. Electromagnetic irradiation-assisted synthesis, exfoliation and modification of graphene-based materials for energy storage and sensing applications. *Mater. Sci. Eng. R Rep.* **2024**, *161*, 100860. [CrossRef]
3. Sahoo, S.; Kumar, R.; Hussain, I.; Zhang, K. Heteroatom doping in 2D MXenes for energy storage/conversion applications. *Adv. Powder Mater.* **2024**, *3*, 100246. [CrossRef]
4. Hemavathi, S.; Srirama, S.; Prakash, A. Present and future generation of secondary batteries: A review. *ChemBioEng Rev.* **2023**, *10*, 1123–1145. [CrossRef]

5. Wu, F.; Liu, M.; Li, Y.; Feng, X.; Zhang, K.; Bai, Y.; Wang, X.; Wu, C. High-mass-loading electrodes for advanced secondary batteries and supercapacitors. *Electrochem. Energy Rev.* **2021**, *4*, 382–446. [CrossRef]
6. Zubair, M.; Hassan, M.M.U.; Mehran, M.T.; Baig, M.M.; Hussain, S.; Shahzad, F. 2D MXenes and their heterostructures for HER, OER and overall water splitting: A review. *Int. J. Hydrogen Energy* **2022**, *47*, 2794–2818. [CrossRef]
7. Qin, D.-D.; Tang, Y.; Ma, G.; Qin, L.; Tao, C.-L.; Zhang, X.; Tang, Z. Molecular metal nanoclusters for ORR, HER and OER: Achievements, opportunities and challenges. *Int. J. Hydrogen Energy* **2021**, *46*, 25771–25781. [CrossRef]
8. Zhang, K.; Zou, R. Advanced transition metal-based OER electrocatalysts: Current status, opportunities, and challenges. *Small* **2021**, *17*, 2100129. [CrossRef]
9. Hansen, J.N.; Prats, H.; Toudahl, K.K.; Mørch Secher, N.; Chan, K.; Kibsgaard, J.; Chorkendorff, I. Is there anything better than Pt for HER? *ACS Energy Lett.* **2021**, *6*, 1175–1180. [CrossRef]
10. Zeng, F.; Mebrahtu, C.; Liao, L.; Beine, A.K.; Palkovits, R. Stability and deactivation of OER electrocatalysts: A review. *J. Energy Chem.* **2022**, *69*, 301–329. [CrossRef]
11. Liang, R.; Du, Y.; Xiao, P.; Cheng, J.; Yuan, S.; Chen, Y.; Yuan, J.; Chen, J. Transition metal oxide electrode materials for supercapacitors: A review of recent developments. *Nanomaterials* **2021**, *11*, 1248. [CrossRef] [PubMed]
12. Sahoo, S.; Wickramathilaka, K.Y.; Njeri, E.; Silva, D.; Suib, S.L. A review on transition metal oxides in catalysis. *Front. Chem.* **2024**, *12*, 1374878. [CrossRef] [PubMed]
13. Deka, S. Nanostructured mixed transition metal oxide spinels for supercapacitor applications. *Dalton Trans.* **2023**, *52*, 839–856. [CrossRef] [PubMed]
14. Pathak, M.; Jeong, S.M.; Rout, C.S. Spinel $NiCo_2O_4$ based hybrid materials for supercapacitors: Recent developments and future perspectives. *J. Energy Storage* **2023**, *73*, 108881. [CrossRef]
15. Wang, Y.; Duan, Y.; Chen, Y.; Zhang, M.; Wang, Y.; Liu, B.; Zhang, X.; Zhang, Y.; Qiu, R.; Yan, K. Facile synthesis of $NiCo_2O_4$ nanosheets efficient for electrocatalysis of water. *Appl. Surf. Sci.* **2024**, *677*, 161013. [CrossRef]
16. Perović, I.M.; Mitrović, S.D.; Brković, S.M.; Pašti, I.A. Advances in Nickel-Based Catalysts for Alkaline Water Electrolysis: Comprehensive Review of Current Research Direction for HER and OER Applications. *Chem. Rec.* **2025**, e202500049. [CrossRef]
17. Wang, Y.-T.; He, X.-F.; He, G.-Y.; Meng, C.; Chen, X.-M.; Li, F.-T.; Zhou, Y. A critical review on nickel sulfide-based electrode materials for supercapacitors. *Crit. Rev. Solid State Mater. Sci.* **2023**, *48*, 502–518. [CrossRef]
18. Chen, Y.; Fan, Y.; Cui, Z.; Huang, H.; Cai, D.; Zhang, J.; Zhou, Y.; Xu, M.; Tong, R. Nickel sulfide-based electrocatalysts for overall water splitting. *Int. J. Hydrogen Energy* **2023**, *48*, 27992–28017. [CrossRef]
19. Qi, Y.; Qiu, L.; Ma, X.; Wu, J.; Xiang, J.; Guo, C.; Yu, J.; Li, K.; Tao, Z.; Lv, Y. Progress in electrocatalytic materials of nickel-based sulfur complexes for HER and OER. *Int. J. Hydrogen Energy* **2024**, *83*, 520–544. [CrossRef]
20. He, R.; Huang, X.; Feng, L. Recent progress in transition-metal sulfide catalyst regulation for improved oxygen evolution reaction. *Energy Fuels* **2022**, *36*, 6675–6694. [CrossRef]
21. Gao, Y.; Zhao, L. Review on recent advances in nanostructured transition-metal-sulfide-based electrode materials for cathode materials of asymmetric supercapacitors. *Chem. Eng. J.* **2022**, *430*, 132745. [CrossRef]
22. Li, J.; Dong, Z.; Chen, R.; Wu, Q.; Zan, G. Advanced nickel-based composite materials for supercapacitor electrodes. *Ionics* **2024**, *30*, 1833–1855. [CrossRef]
23. Chen, X.; Liu, Q.; Bai, T.; Wang, W.; He, F.; Ye, M. Nickel and cobalt sulfide-based nanostructured materials for electrochemical energy storage devices. *Chem. Eng. J.* **2021**, *409*, 127237. [CrossRef]
24. Shahroudi, A.; Esfandiari, M.; Habibzadeh, S. Nickel sulfide and phosphide electrocatalysts for hydrogen evolution reaction: Challenges and future perspectives. *RSC Adv.* **2022**, *12*, 29440–29468. [CrossRef]
25. Sahoo, S.; Kumar, R.; Joanni, E.; Singh, R.K.; Shim, J.-J. Advances in pseudocapacitive and battery-like electrode materials for high performance supercapacitors. *J. Mater. Chem. A* **2022**, *10*, 13190–13240. [CrossRef]
26. Karthikeyan, S.; Narenthiran, B.; Sivanantham, A.; Bhatlu, L.D.; Maridurai, T. Supercapacitor: Evolution and review. *Mater. Today Proc.* **2021**, *46*, 3984–3988. [CrossRef]
27. Kanwade, A.; Shirage, P.M. A review on synergy of transition metal oxide nanostructured materials: Effective and coherent choice for supercapacitor electrodes. *J. Energy Storage* **2022**, *55*, 105692.
28. Zhai, Z.; Zhang, L.; Du, T.; Ren, B.; Xu, Y.; Wang, S.; Miao, J.; Liu, Z. A review of carbon materials for supercapacitors. *Mater. Des.* **2022**, *221*, 111017. [CrossRef]
29. Wang, Y.; Zhang, L.; Hou, H.; Xu, W.; Duan, G.; He, S.; Liu, K.; Jiang, S. Recent progress in carbon-based materials for supercapacitor electrodes: A review. *J. Mater. Sci.* **2021**, *56*, 173–200. [CrossRef]
30. Anil Kumar, Y.; Koyyada, G.; Ramachandran, T.; Kim, J.H.; Sajid, S.; Moniruzzaman, M.; Alzahmi, S.; Obaidat, I.M. Carbon materials as a conductive skeleton for supercapacitor electrode applications: A review. *Nanomaterials* **2023**, *13*, 1049. [CrossRef]
31. Tadesse, M.G.; Ahmmed, A.S.; Lübben, J.F. Review on conductive polymer composites for supercapacitor applications. *J. Compos. Sci.* **2024**, *8*, 53. [CrossRef]

32. Iqbal, M.F.; Ashiq, M.N.; Zhang, M. Design of metals sulfides with carbon materials for supercapacitor applications: A review. *Energy Technol.* **2021**, *9*, 2000987. [CrossRef]
33. Gaikwad, P.; Tiwari, N.; Kamat, R.; Mane, S.M.; Kulkarni, S.B. A comprehensive review on the progress of transition metal oxides materials as a supercapacitor electrode. *Mater. Sci. Eng. B* **2024**, *307*, 117544. [CrossRef]
34. Shaheen, I.; Hussain, I.; Zahra, T.; Javed, M.S.; Shah, S.S.A.; Khan, K.; Hanif, M.B.; Assiri, M.A.; Said, Z.; Arifeen, W.U. Recent advancements in metal oxides for energy storage materials: Design, classification, and electrodes configuration of supercapacitor. *J. Energy Storage* **2023**, *72*, 108719. [CrossRef]
35. Sahoo, S.; Shim, J.-J. Facile synthesis of three-dimensional ternary $ZnCo_2O_4$/reduced graphene oxide/NiO composite film on nickel foam for next generation supercapacitor electrodes. *ACS Sustain. Chem. Eng.* **2017**, *5*, 241–251. [CrossRef]
36. Ding, H.; Liu, H.; Chu, W.; Wu, C.; Xie, Y. Structural transformation of heterogeneous materials for electrocatalytic oxygen evolution reaction. *Chem. Rev.* **2021**, *121*, 13174–13212. [CrossRef]
37. Xiong, Y.; He, P. A review on electrocatalysis for alkaline oxygen evolution reaction (OER) by Fe-based catalysts. *J. Mater. Sci.* **2023**, *58*, 2041–2067. [CrossRef]
38. Li, H.; Lin, Y.; Duan, J.; Wen, Q.; Liu, Y.; Zhai, T. Stability of electrocatalytic OER: From principle to application. *Chem. Soc. Rev.* **2024**, *53*, 10709–10740. [CrossRef]
39. Yan, H.; Zhu, K.; Liu, X.; Wang, Y.; Wang, Y.; Zhang, D.; Lu, Y.; Peng, T.; Liu, Y.; Luo, Y. Ultra-thin NiS nanosheets as advanced electrode for high energy density supercapacitors. *RSC Adv.* **2020**, *10*, 8760–8765. [CrossRef]
40. Liu, X.; Wang, Y.; Luo, C.; Zhang, Z.; Sun, H.; Xu, C.; Chen, H. Hydrothermal synthesis of β-NiS nanoparticles and their applications in high-performance hybrid supercapacitors. *Nanomaterials* **2024**, *14*, 1299. [CrossRef]
41. Wang, J.; Li, S.; Fu, N.; Tian, D.; Zheng, Y.; Wang, F.; Liu, C.; Wang, X.; Zhou, Z.; Niu, Y. MOF-derived carbon-coated NiS/NiS_2 yolk-shell spheres as a satisfactory positive electrode material for hybrid supercapacitors. *Adv. Compos. Hybrid Mater.* **2025**, *8*, 1–12. [CrossRef]
42. Das, A.; Maitra, A.; Mondal, A.; De, A.; Maity, P.; Khatua, B.B. Hydrothermal synthesis of Cu_2S/NiS/Ni_3S_4 as high performance supercapacitor application. *J. Energy Storage* **2024**, *92*, 112293. [CrossRef]
43. Tan, X.; Feng, Z.; Yang, W.; Zou, H.; Chen, S. Flower-like heterogeneous phosphorus-doped Co_3S_4@ Ni_3S_4 nanoparticles as a binder-free electrode for asymmetric all-solid-state supercapacitors. *ACS Appl. Energy Mater.* **2023**, *6*, 702–713. [CrossRef]
44. Wei, W.; Guo, Z.; Qin, X.; Mi, L. Innovative solvent-free compound-direct synthesis of defect-rich ultra-thin NiS nanosheets for high-performance supercapacitors. *Nanoscale* **2024**, *16*, 2522–2530. [CrossRef]
45. Zhang, J.; Zhang, D.; Yang, B.; Shi, H.; Wang, K.; Han, L.; Wang, S.; Wang, Y. Targeted synthesis of NiS and NiS_2 nanoparticles for high–performance hybrid supercapacitor via a facile green solid–phase synthesis route. *J. Energy Storage* **2020**, *32*, 101852. [CrossRef]
46. Wang, H.; Wang, J.; Liang, M.; He, Z.; Li, K.; Song, W.; Tian, S.; Duan, W.; Zhao, Y.; Miao, Z. Novel dealloying-fabricated NiS/NiO nanoparticles with superior cycling stability for supercapacitors. *ACS Omega* **2021**, *6*, 17999–18007. [CrossRef] [PubMed]
47. Shombe, G.B.; Khan, M.D.; Zequine, C.; Zhao, C.; Gupta, R.K.; Revaprasadu, N. Direct solvent free synthesis of bare α-NiS, β-NiS and α-β-NiS composite as excellent electrocatalysts: Effect of self-capping on supercapacitance and overall water splitting activity. *Sci. Rep.* **2020**, *10*, 3260. [CrossRef]
48. Mohapatra, S.; Das, H.T.; Tripathy, B.C.; Das, N. Architecture of Binder-Free Positrodes for Advance Supercapacitors: A Electrodeposited Battery-Type Ternary Cobalt–Nickel–Copper Sulfide. *ACS Appl. Energy Mater.* **2025**, *8*, 1369–1378. [CrossRef]
49. Karmakar, D.A.; Mondal, A.S.; Patra, A.K.; Bhattacharya, S. An Advanced Asymmetric Supercapacitor Electrode Material Based on $Mg(OH)_2$-Ni_3s_4 Nanocomposite. *J. Energy Storage* **2025**, *114*, 115732.
50. Wang, S.; Zhang, P.; Liu, C. Synthesis of hierarchical bimetallic sulfide $NiCo_2S_4$ for high-performance supercapacitors. *Colloids Surf. A Physicochem. Eng. Asp.* **2021**, *616*, 126334. [CrossRef]
51. Amedzo-Adore, M.; Han, J.-I. Surfactant-Assisted $NiCo_2S_4$ for Redox Supercapacitors. *Batteries* **2024**, *10*, 360. [CrossRef]
52. Shwetha, K.; Manjunatha, C.; Kamath, M.S.; Rastogi, C.K.; Chaudhary, V.; Maurya, G.; Athreya, Y.; Shivaraj, B.; Khosla, A. Fabrication of super-high energy density asymmetric supercapacitor prototype device employing $NiCo_2S_4$@ f-MWCNT nanocomposite. *J. Energy Storage* **2023**, *72*, 108657. [CrossRef]
53. He, D.; Li, F.; Xiao, Y.; Chen, S.; Zhu, Z.; Chen, H.; Hu, X.; Peng, W.; Xin, S.; Bai, Y. Electrostatic self-assembly assisted hydrothermal synthesis of bimetallic $NiCo_2S_4$@ N, S co-doped graphene for high performance asymmetric supercapacitors. *Electrochim. Acta* **2022**, *404*, 139751. [CrossRef]
54. Tue, L.N.M.; Sahoo, S.; Dhakal, G.; Nguyen, V.H.; Lee, J.; Lee, Y.R.; Shim, J.-J. $NiCo_2S_4$/MoS_2 nanocomposites for long-life high-performance hybrid supercapacitors. *Nanomaterials* **2023**, *13*, 689. [CrossRef]
55. Van Hoa, N.; Dat, P.A.; Van Hieu, N.; Le, T.N.; Minh, N.C.; Van Tang, N.; Nga, D.T.; Ngoc, T.Q. Rapid and efficient synthesis of high-porous reduced graphene oxide/$NiCo_2S_4$ nanocomposites for supercapacitor application. *Diam. Relat. Mater.* **2020**, *106*, 107850. [CrossRef]

56. Chen, R.; Xue, J.; Gong, Y.; Yu, C.; Hui, Z.; Xu, H.; Sun, Y.; Zhao, X.; An, J.; Zhou, J. Mesh-like vertical structures enable both high areal capacity and excellent rate capability. *J. Energy Chem.* **2021**, *53*, 226–233. [CrossRef]
57. Min, X.; Bo, Z.; Xu, Z.; Feng, J.; Lin, X.; Ni, Y. Porous nanosheet–nanosphere@ nanosheet $FeNi_2$-LDH@ $FeNi_2S_4$ core–shell heterostructures for asymmetric supercapacitors. *Dalton Trans.* **2023**, *52*, 12119–12129. [CrossRef]
58. Guo, Y.; Hao, C.; Yang, Y.; Wu, X.; Ni, C.; Wang, X.; Wang, X. Convenient synthesis of Ni-Mn-S@ rGO composite with enhanced performance for advanced energy storage applications. *Ceram. Int.* **2022**, *48*, 9558–9568. [CrossRef]
59. Cui, Y.; Zhao, C.; Zhao, L.; Yu, H.; Wang, J.; Zhang, Z. Preparation of rGO/Ni_2ZnS_4 and high-performance asymmetric supercapacitors with GO/ZIF-8 template. *Diam. Relat. Mater.* **2022**, *125*, 108965. [CrossRef]
60. Min, X.; Wen, B.; Feng, J.; Lin, X. Nanosheet@ nanosheet $NiZn_2O_4$@$NiZn_2S_4$ core-shell mesoporous heterostructure as an electrode material for aqueous hybrid supercapacitors. *J. Energy Storage* **2024**, *81*, 110410. [CrossRef]
61. Xu, G.; Xu, L.; Zhang, F.; Yu, C.; Song, Y. Facile synthesis of $NiS_{1.03}$@Ni_7S_6/carbon composites with the assistance of biomass resource for supercapacitors with superior electrochemical performance. *Chem. Phys. Lett.* **2024**, *834*, 140969. [CrossRef]
62. Shwetha, K.; Kamath, M.S.; Athreya, Y.N.; Rastogi, C.K.; Nagaraju, K.; Khosla, A.; Manjunatha, C. Development of NiS@f-MWCNT nanocomposite-based high-performance supercapacitor coin cell prototype device. *J. Energy Storage* **2024**, *75*, 109404. [CrossRef]
63. Wu, W.; Yan, Y.; Wang, X.; Wei, C.; Xu, T.; Li, X. Interface construction of CuCoSe@ NiS based on an ultrathin nanosheet for high-performance supercapacitors. *J. Mater. Chem. A* **2024**, *12*, 13818–13829. [CrossRef]
64. Darsara, S.A.; Seifi, M.; Askari, M.B.; Osquian, M. Hierarchical 3D starfish-like Ni_3S_4–NiS on reduced graphene oxide for high-performance supercapacitors. *Ceram. Int.* **2021**, *47*, 20992–20998. [CrossRef]
65. Guo, Y.; Chang, J.; Hu, L.; Lu, Y.; Yao, S.; Su, X.; Zhang, X.; Zhang, H.; Feng, J. Hollow Bowl NiS_2@ polyaniline Conductive Linker/Graphene Conductive Network: A Triple Composite for High-Performance Supercapacitor Applications. *ChemSusChem* **2024**, *17*, e202301148. [CrossRef]
66. Godlaveeti, S.K.; El-marghany, A.; Nagireddy, R.R.; Gedi, S.; Chintaparty, R. Comparative study of electrochemical supercapacitor performance among various nickel phases: Hydroxide, oxide, and sulfide. *Ceram. Int.* **2025**, *51*, 20620–20627. [CrossRef]
67. Narthana, K.; Durai, G.; Kuppusami, P.; Theerthagiri, J.; Sujatha, S.; Lee, S.J.; Choi, M.Y. One-step synthesis of hierarchical structured nickel copper sulfide nanorods with improved electrochemical supercapacitor properties. *Int. J. Energy Res.* **2021**, *45*, 9983–9998. [CrossRef]
68. Alitabar, K.; Zardkhoshoui, A.M.; Hosseiny Davarani, S.S. One-Step Synthesis of Porous Ni–Co–Fe–S Nanosheet Arrays as an Efficient Battery-Type Electrode Material for Hybrid Supercapacitors. *Batter. Supercaps* **2020**, *3*, 1311–1320. [CrossRef]
69. Jinlong, L.; Tongxiang, L.; Meng, Y.; Ken, S.; Hideo, M. Performance comparison of $NiCo_2O_4$ and $NiCo_2S_4$ formed on Ni foam for supercapacitor. *Compos. Part B Eng.* **2017**, *123*, 28–33. [CrossRef]
70. Meng, S.; Wang, Y.; He, J.; Quan, W.; Gao, M.; Jiang, D.; Chen, M. Nanowire-assembled Co_3O_4@NiS core–shell hierarchical with enhanced electrochemical performance for asymmetric supercapacitors. *Nanotechnology* **2020**, *31*, 295403. [CrossRef]
71. Sahoo, S.; Dhakal, G.; Kim, W.K.; Shim, J.-J. Ternary nanohybrid of Ni_3S_2/$CoMoS_4$/MnO_2 on nickel foam for aqueous and solid-state high-performance supercapacitors. *Nanomaterials* **2022**, *12*, 1945. [CrossRef] [PubMed]
72. Reddy, P.A.K.; Han, H.; Kim, K.C.; Bae, S. Heterostructured $NiCo_2S_4$@ SnS_2 hybrid for all-solid-state supercapacitor applications: Delocalized charges on Co–S heterojunction improved electrochemical kinetics. *ACS Appl. Energy Mater.* **2022**, *5*, 13751–13762. [CrossRef]
73. Hu, J.; Pan, Y.; Zhang, Q.; Dong, Z.; Han, S. Constructing flower-shaped $NiCo_2S_4$@CoAl-LDH heterojunction nanosheets exhibits extraordinary electrochemical behavior for a light-assisted asymmetric supercapacitor. *Energy Fuels* **2024**, *38*, 6459–6470. [CrossRef]
74. Cheng, S.; Du, K.; Wang, X.; Han, Y.; Li, L.; Wen, G. Fabrication of Hierarchical MOF-Derived $NiCo_2S_4$@ Mo-Doped Co-LDH Arrays for High-Energy-Density Asymmetric Supercapacitors. *Nanomaterials* **2023**, *13*, 2663. [CrossRef]
75. Cao, J.; Hu, Y.; Zhu, Y.; Cao, H.; Fan, M.; Huang, C.; Shu, K.; He, M.; Chen, H.C. Synthesis of mesoporous nickel-cobalt-manganese sulfides as electroactive materials for hybrid supercapacitors. *Chem. Eng. J.* **2021**, *405*, 126928. [CrossRef]
76. Zhang, Y.; Huang, L.; Lei, X.; Huang, H.; Guo, W.; Wang, S. Hierarchical ternary Zn-Ni-Co sulfide/oxide heterostructure for high specific energy hybrid supercapacitor. *J. Alloys Compd.* **2023**, *962*, 171201. [CrossRef]
77. Ni, S.; Qu, H.; Xing, H.; Xu, Z.; Zhu, X.; Yuan, M.; Rong, M.; Wang, L.; Yu, J.; Li, Y. Interfacial engineering of transition-metal sulfides heterostructures with built-in electric-field effects for enhanced oxygen evolution reaction. *Chin. J. Chem. Eng.* **2022**, *41*, 320–328. [CrossRef]
78. Zhou, N.; Liu, R.; Wu, X.; Ding, Y.; Zhang, X.; Liang, S.; Deng, C.; Qin, G.; Huang, Z.; Chen, B. One-spot autogenous formation of crystalline-amorphous Ni_3S_2/NiFeOxHy heterostructure nanosheets array for synergistically boosted oxygen evolution reaction. *J. Power Sources* **2023**, *574*, 233163. [CrossRef]
79. Shi, Z.; Mao, C.; Zhong, L.; Peng, J.; Liu, M.; Li, H.; Huang, J. Mo-doped Ni_3S_4 nanosheets grown on carbonized wood as highly efficient and durable electrocatalysts for water splitting. *Appl. Catal. B Environ.* **2023**, *339*, 123123. [CrossRef]

80. Prakash, C.; Sahoo, P.; Yadav, R.; Pandey, A.; Singh, V.K.; Dixit, A. Nanoengineered Zn-modified Nickel Sulfide (NiS) as a bifunctional electrocatalyst for overall water splitting. *Int. J. Hydrogen Energy* **2023**, *48*, 21969–21980. [CrossRef]
81. Wang, S.; Yuan, D.; Sun, S.; Huang, S.; Wu, Y.; Zhang, L.; Dou, S.X.; Liu, H.K.; Dou, Y.; Xu, J. Iron, Tungsten Dual-Doped Nickel Sulfide as Efficient Bifunctional Catalyst for Overall Water Splitting. *Small* **2024**, *20*, 2311770. [CrossRef] [PubMed]
82. Qin, J.-F.; Yang, M.; Hou, S.; Dong, B.; Chen, T.-S.; Ma, X.; Xie, J.-Y.; Zhou, Y.-N.; Nan, J.; Chai, Y.-M. Copper and cobalt co-doped Ni_3S_2 grown on nickel foam for highly efficient oxygen evolution reaction. *Appl. Surf. Sci.* **2020**, *502*, 144172. [CrossRef]
83. Mao, X.; Liu, Y.; Chen, Z.; Fan, Y.; Shen, P. Fe and Co dual-doped Ni_3S_4 nanosheet with enriched high-valence Ni sites for efficient oxygen evolution reaction. *Chem. Eng. J.* **2022**, *427*, 130742. [CrossRef]
84. Manjunatha, C.; Srinivasa, N.; Chaitra, S.; Sudeep, M.; Kumar, R.C.; Ashoka, S. Controlled synthesis of nickel sulfide polymorphs: Studies on the effect of morphology and crystal structure on OER performance. *Mater. Today Energy* **2020**, *16*, 100414. [CrossRef]
85. Majeed, M.; Alrowaily, A.W.; Alotaibi, B.; Alyousef, H.A.; Alotiby, M.F.; Khan, M.J.; Hussein, K.I.; Saleem, M.I. Effective OER activity of rhombohedral nickel sulphide nanoparticles supported via reduced graphene oxide. *Diam. Relat. Mater.* **2024**, *148*, 111354. [CrossRef]
86. Li, B.; Li, Z.; Pang, Q.; Zhang, J.Z. Core/shell cable-like Ni_3S_2 nanowires/N-doped graphene-like carbon layers as composite electrocatalyst for overall electrocatalytic water splitting. *Chem. Eng. J.* **2020**, *401*, 126045. [CrossRef]
87. Li, T.; Lu, T.; Li, Y.; Yin, J.; Tang, Y.; Zhang, M.; Pang, H.; Xu, L.; Yang, J.; Zhang, Y. Interfacial engineering-induced electronic regulation drastically enhances the electrocatalytic oxygen evolution: Immobilization of Janus-structured NiS/NiO nanoparticles onto carbon nanotubes/nanofiber-integrated superstructures. *Chem. Eng. J.* **2022**, *428*, 131094. [CrossRef]
88. Yang, X.; Liang, S.; Wang, G.; Zhou, B.; Duan, Z.; Xie, Z.; Hu, Y. Synergistic effect of nanocrystalline $NiCo_2S_4$ and NiCo alloy embedded in N-doped carbon fibers towards high-performance electrocatalysts for oxygen evolution reaction. *J. Alloys Compd.* **2024**, *1007*, 176441. [CrossRef]
89. Lv, Y.; Duan, S.; Zhu, Y.; Yin, P.; Wang, R. Enhanced OER performances of Au@$NiCo_2S_4$ core-shell heterostructure. *Nanomaterials* **2020**, *10*, 611. [CrossRef]
90. Khalid, H.D.; Bilal, A.; Javed, M.; Amjad, A.; Ali, A.; Bahadur, A.; Iqbal, S.; Mahmood, S.; Saleh, T.A.; Rana, A. Sustainable energy generation: High-performance $NiCo_2S_4$@ Sg-C_3N_4 bifunctional electrocatalyst advances water splitting efficiency. *Int. J. Hydrogen Energy* **2024**, *68*, 128–138. [CrossRef]
91. Ke, W.; Zhang, Y.; Imbault, A.L.; Li, Y. Metal-organic framework derived iron-nickel sulfide nanorods for oxygen evolution reaction. *Int. J. Hydrogen Energy* **2021**, *46*, 20941–20949. [CrossRef]
92. Xu, Y.; Sumboja, A.; Groves, A.; Ashton, T.; Zong, Y.; Darr, J.A. Enhancing bifunctional catalytic activity of cobalt–nickel sulfide spinel nanocatalysts through transition metal doping and its application in secondary zinc–air batteries. *RSC Adv.* **2020**, *10*, 41871–41882. [CrossRef]
93. Yang, Y.; Meng, H.; Kong, C.; Yan, S.; Ma, W.; Zhu, H.; Ma, F.; Wang, C.; Hu, Z. Heterogeneous Ni_3S_2@ $FeNi_2S_4$@ NF nanosheet arrays directly used as high efficiency bifunctional electrocatalyst for water decomposition. *J. Colloid Interface Sci.* **2021**, *599*, 300–312. [CrossRef]
94. Wang, C.; Zhu, M.; Cao, Z.; Zhu, P.; Cao, Y.; Xu, X.; Xu, C.; Yin, Z. Heterogeneous bimetallic sulfides based seawater electrolysis towards stable industrial-level large current density. *Appl. Catal. B Environ.* **2021**, *291*, 120071. [CrossRef]
95. He, J.-Z.; Niu, W.-J.; Wang, Y.-P.; Sun, Q.-Q.; Liu, M.-J.; Wang, K.; Liu, W.-W.; Liu, M.-C.; Yu, F.-C.; Chueh, Y.-L. In-situ synthesis of hybrid nickel cobalt sulfide/carbon nitrogen nanosheet composites as highly efficient bifunctional oxygen electrocatalyst for rechargeable Zn-air batteries. *Electrochim. Acta* **2020**, *362*, 136968. [CrossRef]
96. Xu, Y.; Sumboja, A.; Zong, Y.; Darr, J.A. Bifunctionally active nanosized spinel cobalt nickel sulfides for sustainable secondary zinc–air batteries: Examining the effects of compositional tuning on OER and ORR activity. *Catal. Sci. Technol.* **2020**, *10*, 2173–2182. [CrossRef]
97. Wang, X.; Wang, S.; Chen, S.; He, P.; Xu, Y.; Jia, L.; Yang, D.; He, X.; Deng, H.; Jia, B. Facile one-pot synthesis of binder-free nano/micro structured dendritic cobalt activated nickel sulfide: A highly efficient electrocatalyst for oxygen evolution reaction. *Int. J. Hydrogen Energy* **2020**, *45*, 19304–19312. [CrossRef]
98. Chinnadurai, D.; Rajendiran, R.; Kandasamy, P. Bimetallic copper nickel sulfide electrocatalyst by one step chemical bath deposition for efficient and stable overall water splitting applications. *J. Colloid Interface Sci.* **2022**, *606*, 101–112. [CrossRef]
99. Ehsan, M.A.; Khan, A.; Zafar, M.N.; Akber, U.A.; Hakeem, A.S.; Nazar, M.F. Aerosol-assisted chemical vapor deposition of nickel sulfide nanowires for electrochemical water oxidation. *Int. J. Hydrogen Energy* **2022**, *47*, 42001–42012. [CrossRef]
100. Li, T.; Jiang, K.; Li, Y.; Luo, H.; Wang, Z.; Liu, Y.-Q. Crystalline nickel sulfide integrated with amorphous cobalt sulfide as an efficient bifunctional electrocatalyst for water splitting. *Int. J. Hydrogen Energy* **2023**, *48*, 7337–7345. [CrossRef]
101. Dong, W.; Zhou, H.; Mao, B.; Zhang, Z.; Liu, Y.; Liu, Y.; Li, F.; Zhang, D.; Zhang, D.; Shi, W. Efficient MOF-derived V–Ni_3S_2 nanosheet arrays for electrocatalytic overall water splitting in alkali. *Int. J. Hydrogen Energy* **2021**, *46*, 10773–10782. [CrossRef]
102. Ji, X.; Xu, B.; Zhang, H.; Zhang, X.; Yang, P. NiS_2 nanoparticles anchored on Co-carbon nanotubes for supercapacitor and overall water splitting. *J. Alloys Compd.* **2023**, *968*, 172192. [CrossRef]

103. Zhou, B.; Li, J.; Zhang, X.; Guo, J. Engineering P-doped Ni_3S_2-NiS hybrid nanorod arrays for efficient overall water electrolysis. *J. Alloys Compd.* **2021**, *862*, 158391. [CrossRef]
104. Tong, X.; Li, Y.; Pang, N.; Qu, Y.; Yan, C.; Xiong, D.; Xu, S.; Wang, L.; Chu, P.K. Co-doped Ni_3S_2 porous nanocones as high-performance bifunctional electrocatalysts in water splitting. *Chem. Eng. J.* **2021**, *425*, 130455. [CrossRef]

Disclaimer/Publisher's Note: The statements, opinions and data contained in all publications are solely those of the individual author(s) and contributor(s) and not of MDPI and/or the editor(s). MDPI and/or the editor(s) disclaim responsibility for any injury to people or property resulting from any ideas, methods, instructions or products referred to in the content.